Check for updates

Cite as: Z. Zeng *et al.*, *Science* 10.1126/science.ads6055 (2025).

Base-modified nucleotides mediate immune signaling in bacteria

Zhifeng Zeng[1,2]†, Zeyu Hu[1,2]†, Ruiliang Zhao[3]†, Jikai Rao[1,2]†, Mario Rodríguez Mestre[3], Yanqiu Liu[1,2], Shunhang Liu[1,2], Hao Feng[4], Yu Chen[1,2], Huan He[5], Nuo Chen[1,2], Jinshui Zheng[2,6], Donghai Peng[1,2], Min Luo[4], Qunxin She[7], Rafael Pinilla-Redondo[3]*, Wenyuan Han[1,2]*

[1]National Key Laboratory of Agricultural Microbiology, Hubei Hongshan Laboratory, Huazhong Agricultural University, Wuhan, China. [2]College of Life Science and Technology, Huazhong Agricultural University, Wuhan, China. [3]Section of Microbiology, Department of Biology, University of Copenhagen, Copenhagen, Denmark. [4]Center for Bioimaging Sciences, Department of Biological Sciences, National University of Singapore, Singapore. [5]College of Resources and Environment, Huazhong Agricultural University, Wuhan, China. [6]Hubei Key Laboratory of Agricultural Bioinformatics, College of Informatics, Huazhong Agricultural University, Wuhan, China. [7]CRISPR and Archaea Biology Research Center, State Key Laboratory of Microbial Technology, Shandong University, Binhai Road 72, Jimo, Qingdao, China.

†These authors contributed equally to this work.

*Corresponding author. Email: rafael.pinilla@bio.ku.dk (R.P.-R.); hanwenyuan@mail.hzau.edu.cn (W.H.)

Signaling from pathogen sensing to effector activation is a fundamental principle of cellular immunity. While cyclic (oligo)nucleotides have emerged as key signaling molecules, the existence of other messengers remains largely unexplored. Here, we reveal a bacterial anti-phage system that mediates immune signaling through nucleobase modification. Immunity is triggered by phage nucleotide kinases, which, combined with the system-encoded adenosine deaminase, produce deoxyinosine 5′-triphosphate (dITP) as immune messengers. The dITP signal activates downstream effector to mediate cellular NAD$^+$ depletion, resulting in population-level defense through the death of infected cells. To counteract immune signaling, phages deploy specialized enzymes that deplete cellular dAMP, the precursor of dITP messengers. Our findings uncover a nucleobase modification-based anti-phage signaling pathway, establishing noncanonical nucleotides as a new type of immune messengers in bacteria.

Downloaded from https://www.science.org at Shanghai Normal University on February 22, 2025

All cellular life faces constant threats from pathogen invasion, including viruses, driving the evolution of sophisticated immune systems (*1*, *2*). Antiviral systems typically function by relaying pathogen detection to immune effector activation. This signal transduction can occur through mechanisms such as conformational changes or physical interaction of immune components, and the synthesis of signaling molecules (*2*, *3*). Diverse immune pathways have converged on using signaling molecule synthesis due to its advantages in amplifying minimal infection cues and allowing rapid system diversification through sensor and effector swapping (*4*–*6*). Indeed, immune signaling is widespread across prokaryotic and eukaryotic antiviral systems, including the cGAS-STING, OAS-RNaseL, and Toll/interleukin-1 receptor (TIR)-dependent systems in animals and plants (*5*, *7*), as well as the type III CRISPR-Cas (*8*, *9*), CBASS (*10*, *11*), Thoeris (*12*), and Pycsar (*13*) systems in bacteria and archaea. These systems share conceptually similar signal transduction strategies, culminating in the activation of downstream cell death or dormancy effectors that function through diverse mechanisms, including degradation of cellular nucleic acids (*8*, *9*), disruption of membrane integrity (*10*) and depletion of the essential metabolic cofactor NAD$^+$ (*12*). The involved immune signaling molecules are conserved from prokaryotes to animals and plants, typically including cyclic-(oligo)nucleotides and cyclic adenine diphosphate ribose (cADPR) variants. The cADPR variants are generated via processing of NAD$^+$ by TIR domains (*7*, *12*), while nucleotide transferases and cyclases catalyze the synthesis of cyclic-(oligo)nucleotides (*5*, *8*–*11*, *13*). However, the existence of other types of signaling molecules remains unclear.

In this study, we discover and functionally characterize a three-gene bacterial anti-phage defense system. The system specifically produces deoxyinosine 5′-triphosphate (dITP) as an immune signal messenger that activates an immune effector complex to deplete cellular NAD$^+$, leading to population-level protection through the suicide of infected cells. Different from all known immune signaling systems, the three-gene system hijacks phage nucleotide kinases to complete signaling molecule synthesis. We name the three-gene system after Kongming, a great military strategist known in a story “borrowing arrows from enemy”, and designate the three genes *komA*, *komB*, *komC*. Finally, we identify a phage-encoded anti-defense protein that subverts dITP signaling by degrading dAMP, the precursor for dITP synthesis.

Results

Identification of a three-gene anti-phage system

Defense systems tend to cluster in bacterial genomes within “defense islands” (*14*), which provides a powerful strategy to identify new defense systems (*15*–*17*). Through comparative genomics analyses, we identified a three-gene operon that is sometimes located near characterized defense systems (Fig. 1A). This

three-gene system (hereafter Kongming) encodes a predicted adenosine deaminase (pfam PF00962, KomA), a HAM1-like non-canonical purine NTP pyrophosphatase (pfam PF01725, KomB), and a SIR2-like domain-containing protein (pfam PF13289, KomC) (Fig. 1B and figs. S1 and S2). SIR2 proteins are key components of immune systems across all three domains of life (*15*–*19*). These observations led us to hypothesize that Kongming represents a previously uncharacterized defense system. To test this, we cloned the three-gene operon from *Escherichia coli* NCTC13216 under the control of its native promoter into the pET28a plasmid. Expression of Kongming in *E. coli* MG1655 challenged with a panel of coliphages revealed strong immunity against a wide range of phages (Fig. 1C and fig. S3). Next, we investigated whether Kongming provides immunity at the population level, a defense strategy that only protects bacterial culture at a low multiplicity of infection (MOI < 1), i.e., the ratio of phages to host cells less than 1 (*20*). We infected the liquid cultures expressing Kongming with phage Rao1 at MOI of 3 and 0.3. Kongming rescued culture growth only at a MOI of 0.3, whereas infection at an MOI of 3 resulted in a premature growth retardation (Fig. 1D and fig. S4). The data suggest that Kongming provides population-level immunity.

To investigate whether each of the three components is essential for anti-phage immunity, we assayed mutated versions of the system. Alanine substitution of the conserved residues within the active site pocket of KomA (His15, His17) (*21*) and KomC (His146) (*22*) (fig. S2) abolished the immune defensive phenotype against Rao1 (Fig. 1E and fig. S5), indicating that the enzymatic activities of KomA and KomC are essential for Kongming defense. In contrast, the conserved catalytic aspartic acid, responsible for nucleophilic attack in experimentally characterized HAM1 family enzymes (*23*), is replaced by histidine in KomB (His65) (fig. S2), suggesting that KomB may be catalytically inactive. Nevertheless, KomB retains the conserved residues that are implicated in binding to non-canonical purine NTP substrates in its experimentally characterized homologs (*23*) (fig. S2). Alanine substitution of three substrate-binding residues (Asn9, Lys12, and Glu15) also abrogated immunity (Fig. 1E and fig. S5), underscoring that the binding of KomB to non-canonical purine NTP is required. Together, the data indicate that Kongming is an anti-phage system, where each of the three components plays an indispensable role.

Phage DNKs trigger Kongming immunity

Phages often evolve resistance to bacterial immune defenses by acquiring mutations in the components sensed by the immune systems, thereby providing valuable insights into the system's activation mechanism (*24*, *25*). To identify potential phage-encoded triggers, we infected *E. coli* cells expressing Kongming with Rao1 and isolated immune escaper mutants for further examination (Fig. 1F). We found that the escapers all carried mutations within the coding sequence or promoter region of the gene *gp58* (Fig. 1F and table S5), which encodes a phage deoxynucleotide monophosphate kinase (hereafter, R1DNK) (fig. S6A). To investigate whether R1DNK acts as the trigger of Kongming, we analyzed the cell viability and culture growth kinetics of cells co-expressing R1DNK and Kongming (Fig. 1G and fig. S7A). Co-expression induced extensive cell death and growth suppression, suggesting that R1DNK alone triggers Kongming toxicity. Furthermore, the toxicity was eliminated when the conserved catalytic residue Lys^{15} of R1DNK was mutated to alanine (K15A), indicating that the enzymatic activity of R1DNK is essential for triggering the Kongming immunity (Fig. 1G and figs. S7, A and B, and S5).

Phage DNKs can catalyze the phosphorylation of dNMP or modified dNMP to the corresponding dNDP, which are then converted to dNTPs for rapid phage genome replication (fig. S6A) (*26*, *27*). To investigate the function of R1DNK, we constructed a *dnk* deletion Rao1 mutant ($Rao1^{\Delta dnk}$) using CRISPR-Cas13 (*28*). The mutant was resistant to Kongming, reinforcing that R1DNK is the trigger (fig. S8A). Infection with Rao1 induced a gradual ~two- to threefold increase in the dAMP, dADP and dATP levels (fig. S8B). Deletion of *dnk* resulted in a moderately lowered dATP level, indicative of a role of R1DNK in phage dNTP synthesis (fig. S8B). Nevertheless, the phage competition assay indicates that deletion of *dnk* did not cause apparent fitness cost, implying that the DNK-mediated dNTP synthesis is not critical for Rao1 replication under our experimental conditions (fig. S8C).

Phylogenetic analysis revealed that DNKs are widely distributed across phages belonging to distinct families (Fig. 1H and fig. S7C), consistent with the broad protective activity of Kongming. To test if Kongming is activated by other phage DNKs, we selected six representative DNK homologs from different branches of the phylogenetic tree and co-expressed them with Kongming. The DNKs from T5 phage, Klebsiella phage vB_KpnS-VAC2, Vibrio phage XZ1, and Escherichia phage KarlJaspers triggered Kongming toxicity (Fig. 1H and fig. S7D). In contrast, the DNK from Bacillus phage vB_BsuM-Goe24 or Erwinia phage FIfi106 did not induce Kongming-mediated cell death (Fig. 1H and fig. S7D), suggesting that these DNKs either have distinct enzymatic properties, or we could not recapitulate their activity through heterologous expression in *E. coli*. We found that the distribution of DNKs in our tested phage collection correlates well with the Kongming immunity, except for a minority of phages (fig. S3). These results support the notion that Kongming is triggered by phage-encoded DNKs or their enzymatic activities. Notably, within the exceptions of DNK-encoding phages, T5-like phages are particularly resistant to Kongming (Fig. 1C). However, expression of T5DNK in the absence of infection robustly activates Kongming toxicity (fig. S7D), suggesting that T5-like phages encode anti-Kongming factors. On the other hand, a few phages that are sensitive to Kongming do not encode DNK (fig. S3), indicating that Kongming might be triggered by remote DNK homologs that are not detected in this study or through alternative mechanisms that require further

Downloaded from https://www.science.org at Shanghai Normal University on February 22, 2025

investigation.

KomB and KomC form an effector complex capable of NAD$^+$ degradation

In various SIR2-containing anti-phage systems, such as Thoeris, defense-associated sirtuins (DSRs) and SIR2-containing pAgo systems, SIR2 acts as the cell-killing effector module via rapid cellular NAD$^+$ depletion (*12*, *29*, *30*). To test whether KomC similarly degrades NAD$^+$, we measured NAD$^+$ levels in the cells co-expressing R1DNK and Kongming (Fig. 2A). Indeed, co-expression resulted in significant NAD$^+$ depletion, and mutation in the active site of KomC abrogated this activity, confirming that KomC is responsible for NAD$^+$ degradation. The NAD$^+$ depletion was accompanied by extensive cell death (fig. S7E), in line with our previous observations (Fig. 1G). The observed NAD$^+$ depletion was also abrogated when KomA, KomB, or R1DNK was mutated in their respective conserved sites, indicating that the activation of KomC is dependent on the activities of KomA and R1DNK and the substrate-binding ability of KomB.

To investigate whether KomC activation requires effector complex formation, we examined its potential interactions with KomA, KomB, or R1DNK. We co-expressed R1DNK and Kongming, where KomC carried a 6XHis tag to allow Ni-NTA affinity purification and a H146A mutation to abolish its toxic NADase activity (fig. S9A). The co-purified proteins were subjected to mass spectrometry (MS) analysis. Compared to the control purification with untagged KomC^{H146A}, KomB and KomC were substantially enriched in the purification with His-tagged KomC^{H146A} (Fig. 2B, fig. S9B, and table S6), indicating a physical interaction between KomB and KomC. SDS–polyacrylamide gel electrophoresis (PAGE) and MS analysis confirmed that both KomB and KomC were retrieved by Ni-NTA affinity purification from cells co-expressing KomB and His-tagged KomC, reinforcing the notion that the two proteins form a stable complex (Fig. 2C, fig. S9C, and table S7). Additionally, pull-down experiments using maltose binding protein (MBP) tagged KomA and Strep-tagged R1DNK did not detect any interaction between KomA and KomBC complex or between the phage-encoded trigger and the three proteins of Kongming (fig. S9, D and E), suggesting that R1DNK activates Kongming indirectly rather than through protein-protein interaction.

We then analyzed whether KomC, standalone or in the complex with KomB, has NADase activity using ε-NAD as substrate, the degradation of which produces a fluorescent product (Fig. 2D). The KomBC complex efficiently degraded ε-NAD in the presence of Zn^{2+}, whereas KomC alone did not cleave ε-NAD in the same condition (Fig. 2E and fig. S10A), underscoring the requirement of complex formation with KomB for the NADase activity. Analysis of the NAD$^+$ degradation products indicates that KomBC degraded NAD$^+$ into nicotinamide (NAM) and ADP-ribose (ADPR), in line with the products of the SIR2 effectors in other defense systems (*12*, *29*) (Fig. 2F). Further, the NADase activity was abrogated by the mutation of the KomC active site but not affected by the mutation of KomB (Fig. 2G and fig. S10B), confirming that the active site of KomC catalyzes the degradation of NAD$^+$. Taken together, these results demonstrate that KomB and KomC form the effector complex that is responsible for immune NAD$^+$ depletion.

dITP activates the KomBC effector complex

The observation that neither R1DNK nor KomA physically interact with the KomBC complex, despite their activities being essential for triggering NAD$^+$ degradation, led us to speculate that KomA and R1DNK activate KomBC via synthesizing a second messenger. The predicted functions of KomA, R1DNK, and KomB are linked to nucleotide metabolism pathways, suggesting that Kongming could rely on a previously unrecognized nucleotide-based immune messenger. Given that KomB forms a stable complex with KomC (Fig. 2C) and has a mutated catalytic site (fig. S2), we hypothesized that KomB may function as a signal recognition module. Additionally, previously characterized KomB family proteins, known as inosine triphosphate pyrophosphatases (ITPases), are house-keeping enzymes that hydrolyze noncanonical nucleoside triphosphates to prevent their incorporation into nascent DNA and RNA chains, e.g., degrading ITP and dITP to IMP and dIMP, respectively (*23*, *31*). Together, these observations suggest that the putative signaling molecule could be a noncanonical nucleotide.

To test this idea, we analyzed the NADase activity of KomBC in the presence of dITP, ITP, IDP, IMP, dUTP, or canonical nucleotides (dNTPs and NTPs). The results show that dITP activates the NADase activity of KomBC most robustly (Fig. 3A). While IDP also activated KomBC, it triggered a >100-fold weaker response compared to dITP, and the other tested nucleotides did not activate KomBC (Fig. 3A and fig. S10, C and D). Upon activation, the NADase activity generated the same products as those in the absence of dITP (fig. S10E). These findings indicate that dITP is the signaling molecule that activates KomBC for NAD$^+$ degradation. Furthermore, the KomBC complex with inactive KomC did not exhibit any NADase activity, whereas the KomB mutation still retained the basal activity but abolished the dITP-stimulated activity (Figs. 2G and 3B). To test whether KomBC degrades the dITP immune signal, which may represent an autoinhibition mechanism observed in type III CRISPR-Cas system signaling pathways (*32*), we incubated dITP with KomBC and analyzed the potential products (fig. S10F). However, no products were detected, indicating that KomB has lost its dITP pyrophosphatase activity. Together, these results indicate that KomB functions as the signal-recognition module that senses dITP as an immune signal and mediates activation of KomC.

Kongming and R1DNK produce dITP signaling molecules in vivo

Downloaded from https://www.science.org at Shanghai Normal University on February 22, 2025

We next analyzed whether Kongming synthesizes the signaling molecule dITP in response to phage infection in vivo. We hypothesized that the synthesized signal could be bound by KomBC. Therefore, to retrieve the putatively bound molecule, we purified the KomBC^{m} complex (C^{m}, KomC^{H146A}) from cells expressing His-tagged KomC^{m}, KomA, KomB, and the phage trigger R1DNK (Fig. 3C and fig. S11A). The purified KomBC^{m} complex was subsequently denatured and precipitated, and the resulting supernatant was analyzed by liquid chromatography–tandem mass spectrometry (LC-MS/MS) to investigate whether it contains dITP (Fig. 3, D to F). The analysis detected a molecule that has the same retention time, mass/charge (m/z) value, and molecular fragments as dITP. In addition, the molecule was absent in the KomBC complex purified from the cells containing a mutated KomA or R1DNK, or in the KomB^{m}C complex (B^{m}, KomB$^{N9A\text{-}K12A\text{-}E15A}$) from the cells containing wild-type KomA and R1DNK (Fig. 3E). The data suggest that KomBC binds to dITP as a signaling molecule and that the enzymatic activities of both KomA and R1DNK are required for dITP synthesis in vivo.

To explore whether the dITP in the supernatant activates KomBC, we measured the concentration of the released dITP via LC-MS/MS (fig. S11B), diluted it to the same dITP concentation as the standard, and analyzed its capability to activate KomBC (Fig. 3G). The results revealed similar activation efficiency of the diluted supernatant and the dITP standard. In addition, the supernatant from the cultures with mutation in KomA, R1DNK or KomB failed to activate KomBC (fig. S11C). Together, these results confirm that dITP is the sole signaling molecule synthesized by Kongming in response to phage DNK and recognized by KomBC for immune activation.

Biosynthetic pathway of the dITP immune signal

To reveal how dITP is synthesized during the immune response, we characterized the biochemical properties of KomA and R1DNK, which are shown essential for dITP synthesis (Fig. 3E). Given that characterized homologs of KomA catalyze deamination of adenosine and deoxyadenosine to inosine and deoxyinosine, respectively (Fig. 4A) (*33*), we tested the substrate specificity of KomA against diverse adenine nucleotides. Incubation with dAMP, dADP, dATP, AMP, ADP, or ATP, followed by the analysis of the resulting products via high-performance liquid chromatography (HPLC) revealed that KomA shows the highest adenosine deaminase activity with dAMP as a substrate and produces dIMP, whereas the deamination of dADP, AMP, and ADP were also observed (Fig. 4B and fig. S12). Nevertheless, deamination of dATP was not detected (Fig. 4B), suggesting that KomA cannot complete dITP production by itself, which possibly requires a factor that becomes available during phage infection.

Therefore, we hypothesized that Kongming hijacks the phage DNKs to produce dITP. Phage DNKs are supposed to phosphorylate dNMP to dNDP (fig. S6A) (*26*, *27*), which are then converted to dNTPs by host nucleoside diphosphate kinases (NDKs) (*34*) to facilitate phage genome replication (Fig. 4C). Biochemical characterization of R1DNK showed that R1DNK efficiently phosphorylated dAMP, dGMP and dCMP to dADP, dGDP, and dCDP, respectively, and also showed kinase activity with dTMP as a substrate (Fig. 4D and fig. S13). However, the conversion of dIMP to dIDP was minimal (Fig. 4D). Together, the data suggest that KomA and R1DNK can catalyze a cascade reaction to produce dIDP from dAMP.

To explore how KomA and R1DNK produce dITP in vivo, we analyzed the levels of adenine nucleotides and their inosine derivatives in cells expressing R1DNK and Kongming carrying a KomC^{H146A} mutation (KomABC^{m}). The cells expressing KomABC^{m} accumulated dIMP but not dIDP or dITP, indicating that KomA only deaminates the host dAMP (Fig. 4E). Expression of R1DNK resulted in elevated dADP level, confirming its capability to phosphorylate dAMP (Fig. 4E). In the cells co-expressing R1DNK and KomABC^{m}, dITP, the final signaling molecule, was accumulated, while dIDP was still not detectable (Fig. 4E). These results suggest that dIDP can be rapidly converted to dITP. In addition, compared to expression of KomABC^{m} alone, co-expression of R1DNK and KomABC^{m} resulted in lowered dIMP level, implying that R1DNK may phosphorylate dIMP in vivo.

To investigate whether host NDK can convert dIDP to dITP, we sought to reconstitute the cascade reaction of dITP production. We first incubated dADP with KomA, and then with *E. coli* NDK and ATP, and analyzed the product for its ability to activate KomBC (Fig. 4F). As expected, the product efficiently activated KomBC for NAD^{+} degradation (Fig. 4F). LC-MS/MS analysis confirmed that the product contained dITP (fig. S14, A and B). In addition, the absence of either KomA or NDK abolished dITP generation, indicating that NDK is a host enzyme involved in dITP synthesis (Fig. 4F and fig. S14A). Next, we incubated dIMP with R1DNK and ATP, and then with NDK. The resulting product also activated KomBC (Fig. 4G). Further, using LC-MS/MS, we detected dIDP as the product after incubation of dIMP with R1DNK and ATP (fig. S14C-E). The data indicate that R1DNK indeed harbors the dIMP phophorylation activity, although LC failed to detect the product (Fig. 4D). Collectively, the results establish that KomA and R1DNK can generate dIDP from dAMP and that host NDK converts the generated dIDP to dITP as the signaling molecule. The dIDP can be generated through two pathways (fig. S14F): (i) phosphorylation of dAMP by R1DNK followed by deamination of dADP by KomA and (ii) dAMP deamination by KomA followed by phosphorylation of dIMP by R1DNK. Both the two pathways may contribute to immune signaling in vivo, while the specific extent of the contribution of each pathway might be dependent on the phage DNK substrate specificity and nucleotide metabolism mechanism.

Phage-encoded inhibitor of Kongming immunity

Our observation that T5 is resistant to Kongming, despite the

Downloaded from https://www.science.org at Shanghai Normal University on February 22, 2025

robust triggering of Kongming by T5DNK expression, led us to hypothesize that T5 encodes an anti-Kongming factor (Fig. 1C and fig. S7D). In other anti-phage signaling systems, such as CBASS, Thoeris, and type III CRISPR-Cas, phages typically counteract immunity by targeting the signaling molecule, either by sponging it or leading to its degradation (*35*–*38*). We therefore hypothesized that T5 may encode an anti-Kongming factor with dITP-binding or -processing ability. Previous studies have shown that T5 encodes a deoxyribonucleotide 5′ monophosphatase (T5Dmp) that converts 5′-dNMP to deoxynucleosides before phage genome replication begins (*39*). We hypothesized that it may subvert Kongming immunity by degrading dAMP, the precursor for dITP synthesis. To confirm this, we constructed a *dmp* deletion T5 mutant ($T5^{\Delta dmp}$) and analyzed the sensitivity of $T5^{\Delta dmp}$ to Kongming. Compared to wild-type T5, $T5^{\Delta dmp}$ could not overcome Kongming immunity, indicating that T5Dmp indeed functions as an anti-Kongming factor (Fig. 5A). Analysis of nucleotides levels post infection shows that wild type T5 resulted in lowered dAMP level at 5 min, while $T5^{\Delta dmp}$ induced a sharp accumulation of dAMP (Fig. 5B), confirming that T5 infection degrades the host genome into dNMP, while T5Dmp is responsible for depletion of cellular dNMP (*39*). Moreover, dAMP accumulation post $T5^{\Delta dmp}$ infection was accompanied with elevated dADP and dATP levels, indicative of efficient phosohorylation of dAMP to these nucleotides (Fig. 5B).

We further examined the phosphatase activity of T5Dmp and, in line with previous studies (*40*), T5Dmp displayed phosphatase activity with dNMP substrates, as well as dIMP and dADP, but failed to degrade dITP (fig. S15, A andB). These results indicate that the anti-Kongming function of T5dmp is not achieved by the degradation of the signaling molecule. To confirm the dependency of T5Dmp's anti-Kongming function on its enzymatic activity, we constructed a T5Dmp mutant that carries an alanine substitution at D22, a conserved residue in phosphatases that functions in Mg^{2+} coordination (fig. S15C) (*41*). Indeed, compared to wild-type T5Dmp, the D22A mutant showed no phosphatase activity with dAMP as substrate (Fig. 5C). Consistently, the D22A mutation abolished the ability of T5Dmp to protect Rao1 from Kongming immunity, suggesting that T5Dmp's phosphatase activity is required for its anti-defense function (Fig. 5D). To investigate whether T5Dmp inhibits Kongming by interfering the DNK-triggered signaling pathway, we cloned T5Dmp into the cells co-expressing T5DNK and Kongming. Here, T5Dmp suppressed the Kongming immunity-triggered cell death, while the D22A mutation restored the immunity (Fig. 5E). Together, our data collectively indicate that T5Dmp is a robust anti-Kongming inhibitor that functions via removal of cellular dAMP, the precursor for dITP synthesis (Fig. 5F).

To further explore the functional impact of T5Dmp and T5DNK, we compared the fitness of wild type T5 and T5 mutants carrying *dmp* and *dnk* deletions via phage competition assays. This revealed that deletion of *dmp* resulted in severe fitness cost (fig. S16A). Deletion of *dnk* also induced fitness defects in both wild type T5 and $T5^{\Delta dmp}$ (fig. S16A). The results suggest that T5DNK and T5Dmp play important roles in the phage replication cycle. Notably, T5 encodes its own de novo nucleotide synthesis pathways (*42*), which might involve the DNK activity. In addition, infection with $T5^{\Delta dmp\text{-}dnk}$ still induced accumulation of dADP and dATP, suggesting an alternative dAMP phosphorylation mechanism (fig. S16B). Consistently, the $T5^{\Delta dmp\text{-}dnk}$ phage was sensitive to Kongming, indicating that DNK is not the sole trigger (fig. S16C). Taken together with the phenotypes of Rao1, our data indicate that T5 and Rao1 encode distinct nucleotide metabolism pathways, with their DNKs likely adapted to different functions (fig. S6).

Phylogenetic analysis of Dmp homologs across phages revealed their frequent co-existence with DNKs (Fig. 5G and fig. S17), reinforcing their function as anti-Kongming proteins that prevent Kongming immune activation by phage DNKs. To further investigate this hypothesis, we selected three additional Dmps and tested their ability to inhibit the toxicity from the co-expression of DNK and Kongming. Two of them originate from distantly related phages not present in our tested panel (Erwinia phage KEY and Vibrio phage VPG01), and the third one is from Bas26, a phage shown to be sensitive to Kongming immunity (fig. S3). While we were unable to construct the expression plasmid for Erwinia phage KEY Dmp (probably due to its toxicity in *E. coli*), the Dmps from Vibrio phage VPG01 and Bas26 robustly suppressed cell death triggered by Kongming and their respective DNKs (figs. S15D and S17), indicating their anti-Kongming function. The reason why Bas26 is still sensitive to Kongming (fig. S3) given that it encodes a functional anti-Kongming factor is unknown and requires further investigation.

Distribution and genetic associations of Kongming components

Given that previously studied HAM1 family proteins are recognized housekeeping enzymes implicated in the removal of non-canonical nucleotides in cells (*23*, *31*), we asked whether defense-associated HAM1 proteins represent a specialized subfamily adapted to immune functions. To address this question, we conducted a phylogenetic analysis of a diverse set of 154,151 HAM1 proteins, with representatives from all three domains of life. The analysis revealed that known housekeeping HAM1 proteins are scattered across many clades of the tree, yet excluded from the distinct clade including KomB (hereafter defensive HAM1 clade) (Fig. 6A). Notably, compared to a clade with housekeeping HAM1s (non-defensive clade), members of the defensive HAM1 clade are frequently located near known anti-phage systems and within plasmid and prophage elements, further supporting their immune function (Fig. 6B). Furthermore, the defensive HAM1s invariably carry the histidine substitution of the catalytic aspartic acid residue that is conserved in non-defensive HAM1s (Fig. 6C).

Downloaded from https://www.science.org at Shanghai Normal University on February 22, 2025

On the other hand, the defensive HAM1s retain the conserved non-canonical nucleotide-binding residues that constitute the substrate-binding pocket in the housekeeping HAM1s (Fig. 6, C and D, and fig. S18). Together, the data suggest that the defensive HAM1 has evolved from active pyrophosphatases to catalytically dead proteins that function as the signal-sensing module.

Bacterial defense systems rapidly diversify to keep pace with counter-evolving phages by swapping effector and sensor components (*43*). The typical modular architecture of defense systems led us to hypothesize that defensive HAM1s might associate with other proteins to form defense systems beyond Kongming. To investigate this, we analyzed the phylogenetic tree of defensive HAM1s and searched for HAM1-associated proteins. Defensive HAM1s can be classified into two major clades and several subclades that have different association protein patterns (Fig. 6E and fig. S19). Defensive HAM1s from all clades are tightly associated with KomC (Fig. 6E and fig. S19), implying that the immune function of HAM1 is likely due to its functional association with SIR2-like effectors. Indeed, we observed a strong co-evolutionary signal between genetically associated KomB and KomC (Fig. 6F), with instances of these domains being fused into a single protein (fig. S19A, candidate type 4). These observations are in line with that the two proteins form a stable complex (Fig. 2, B and C). In contrast, neither of these genes showed a comparable correlation with the evolutionary distances of the host 16S ribosomal RNA (rRNA) sequences, suggesting that the KomBC module frequently spreads horizontally (Fig. 6F). Together, these results indicate that the KomBC association has remained stable across evolutionary timescales, coupling the immune sensing of second messengers to KomC activation.

By comparison, the association between defensive HAM1 and KomA appears less conserved. In the absence of KomA, we identify various proteins that appear to be genetically associated with the KomBC module (Fig. 6E and fig. S19). Notably, these instances often include proteins involved in nucleotide metabolism or modification (e.g., 5′-nucleotidase, uracil-DNA glycosylase, NTPase, and SAM-dependent methyltransferase), suggesting a conserved function in the generation of dITP or other nucleotide-based immune signaling molecules to activate the KomBC effector (fig. S19A). We found associated RADAR-like systems that may functionally synergize with KomBC by serving as sensor modules, with RdrB harboring an adenosine deaminase domain that is known to drive the massive production of ITP and dITP molecules (fig. S19A) (*44*, *45*). Although the ability of these genetically associated modules to activate KomBC needs further investigation, their common presence in mobile genetic elements and within defensive genomic contexts strongly suggests their antiviral function. (fig. S19B). Overall, the diversity of bacterial operons containing KomBC modules and other proteins indicates that various (sub)types of Kongming are widespread across bacteria, reflecting that the modularity of the bacterial immune systems enables their rapid diversification in the arms race with phages.

Discussion

In this study, we discover and characterize the Kongming antiphage system, which mediates an immune signaling pathway based on the production of deoxyinosine 5′-triphosphate (dITP) as a second messenger. In contrast to previously characterized immune signaling pathways using cyclic (oligo)nucleotides and ADPR-derived signals (*5*, *7–12*, *46–48*), Kongming generates the noncanonical nucleotide dITP through a cascade reaction including base modification and nucleotide phosphorylation.

The synthesis of the dITP signal involves three enzymes, including the adenosine deaminase of Kongming (KomA), phage dNMP kinases (DNKs), and a host dNDP kinase (NDK). KomA and phage DNKs can synthesize dIDP from dAMP via two pathways, subsequently followed by NDK-mediated conversion of the generated dIDP to dITP (Fig. 5F). The two alternative pathways might enable Kongming to defend against a wide range of phages while avoiding self-toxicity. Different phage DNKs may have distinct substrate specificities, probably with weak dIMP phosphorylation activity, as dIMP is not a natural substrate for phage dNTP synthesis. Thus, to efficiently trigger immune signaling, KomA exhibits a relatively high dAMP deamination activity. Notably, since dAMP is not a precursor of host dATP synthesis (fig. S6B) and dIMP can be recycled via purine salvage pathway (fig. S6C) (*34*), dAMP deamination is not toxic for cells. On the other hand, deamination of host dADP is lethal because the generated dIDP can be rapidly converted to dITP, triggering the immune response. Therefore, the dADP deamination activity of KomA should be weak to avoid self-toxicity. In addition, the host dADP is generated via reduction of ADP by ribonucleotide reductase (RNR) (fig. S6B), the activity of which is tightly regulated (*34*). Such regulation might protect host dADP from KomA deamination, ensuring that only phage-generated dADP serves as the immune trigger.

Once synthesized, dITP specifically activates the KomBC complex for rapid depletion of the cellular NAD^+ pool, resulting in the death of infected cells and population-level immunity (Fig. 5F). Within the KomBC complex, the KomC subunit, which contains a SIR2-like domain, functions as the NAD^+-degrading effector module. NAD^+ depletion is observed across several immune system families, highlighting a diversity of mechanisms coupling viral sensing to SIR2 effector activation (*12*, *29*, *30*). KomB mediates KomC activation through recognition of the dITP signal, using a catalytically dead HAM1-like domain. While active HAM1-like enzymes are housekeeping pyrophosphatases of non-canonical nucleotides, catalytically dead HAM1-like proteins are found exclusively associated to Kongming-like systems (Fig. 6). This suggests that KomB evolved from a housekeeping enzyme into a dedicated immune signal sensor.We reveal that T5-like phages encode deoxyribonucleotide 5′ monophosphatase (Dmp) enzymes that counteract Kongming immunity (Fig. 5F). Notably,

Downloaded from https://www.science.org at Shanghai Normal University on February 22, 2025

during the infection cycle of T5, the genomic region encoding Dmp is injected into cells first, resulting in early expression of the enzyme and depletion of cellular dAMP pool (Fig. 5B) (*39*, *49*). Afterwards, the rest of the phage genome, including the *dnk* gene, is injected into cells, and phage genome replication is initiated (*39*), with all required nucleotides synthesized de novo (fig. S6D) (*42*). This time-resolved expression of Dmp and DNK may completely avoid dITP synthesis, thereby preventing Kongming activation. In support of this notion, Dmps are primarily distributed in phages that also carry DNKs. Together, these findings reveal a defense and anti-defense arms race for the control of the host's nucleotide metabolism.

Given that several key components of the eukaryotic innate immune system originate from ancient bacterial immune components (*50*), our findings raise the question as to whether dITP or other non-canonical nucleotides may participate in immune signaling across domains of life. Non-canonical nucleotides are indeed produced in eukaryotic cells through spontaneous deamination (*51*). Furthermore, since the KomBC effector complex specifically responds to dITP, it could serve as a tool for detecting this non-canonical nucleotide, which can be accumulated due to mutation of ITPase and incorporated into DNA during replication, leading to genome instability, cancer, and other diseases (*51*, *52*).

Materials and Methods

Bacterial strains and phages

E. coli DH5α and *E. coli* BL21(DE3) were used for plasmid construction and protein expression, respectively. *E. coli* strains MG1655, PC0886 and ER2738 were used as hosts for phage-related experiments. DH5α and BL21(DE3) were grown in lysogeny broth (LB) medium at 37°C shaking at 180 rmp. The strains used for phage experiments were grown in MMB medium (LB supplemented with 0.1 mM $MnCl_2$, 5 mM $MgCl_2$) at 37°C shaking at 180 rmp. When appropriate, the media were supplemented with kanamycin (50 μg/ml), streptomycin (50 μg/ml), ampicillin (100 μg/ml) and/or chloramphenicol (25 μg/ml) to maintain the plasmids. All phages used in this study and their respective hosts are listed in table S4. Rao1 phage is a gift from Prof. Shuke Wu at Huazhong Agricultural University and sequenced in this study. Phages of BASEL collection are a gift from Dr. Alexander Harms at University of Basel (*53*).

Plasmid construction

The plasmids vectors used in this study and the constructed plasmids are listed in table S2. To express the proteins of interest (table S1), their coding sequences, sometimes together with their native promoters as indicated, were amplified from phage or *E. coli* genomic DNA, or synthesized by GENEWIZ (Suzhou, China). In general, the plasmids were constructed with ClonExpress II One Step Cloning Kit (Vazyme, C112-02) or restriction-ligation cloning method as described previously (*30*). Site-directed mutagenesis was performed by PCR amplification of the plasmids carrying the intact genes using the primers containing mutant sites, followed by assembly of the resulting plasmid fragments in *E. coli* DH5α. The primers used in the study are listed in table S3.

The KomABC system, together with its native promoter, was synthesized and inserted into the pET28a plasmid between the BglII and XhoI sites by GENEWIZ (Suzhou, China), resulting in pET28a-KomABC. The plasmids encoding mutated KomABC systems, including pET28a-A^{m}HS, pET28a-KomAB^{m}C and pET28a-KomABC^{m}, were constructed by the site-directed mutagenesis method using primers from ZZF-36 to ZZF-41. The KomABC system with its native promoter and the mutated variants were also cloned into the pCDFDuet-1 vector, generating pCDF-KomABC, pCDF-KomA^{m}BC, KomAB^{m}C and pCDF-KomABC^{m} respectively.

To express R1DNK, the coding sequence of R1DNK was amplified from Rao1 phage genomic DNA using primers ZZF-5 and ZZF-6, and then inserted into pBAD/His_A plasmid between the NcoI and HindIII sites, generating pBAD-R1DNK. The plasmid encoding R1DNK mutant (pBAD-R1DNK^{K15A}) was constructed by the site-directed mutagenesis method using primers ZZF-42 and ZZF-43. The pBAD/His_A-derived plasmids expressing other DNKs were constructed in a similar way. The coding sequences of T5DNK and Escherichia phage KarlJaspers (MZ501090) DNK were amplified from the genomic DNA of the corresponding phages, while the coding sequences of the DNKs from Klebsiella phage vB_KpnS-VAC2 (MZ428221), Bacillus phage vB_BsuM-Goe24 (OM728302), Erwinia phage FIfi106 (OR284297) and Vibrio phage XZ1 (ON000910) were synthesized and inserted into the pBAD/His_A plasmid between NcoI and HindIII sites by GENEWIZ (Suzhou, China).

We constructed a pBAD-Tag vector by inserting the sequence encoding an N-terminal 3× Myc-tag and a C-terminal 3× Flag-tag into pBAD/His_A. The plasmids pBADT-KomA (containing an N-terminal 3× Myc-Tag), pBADT-KomA^{m} (containing an N-terminal 3× Myc-Tag), pBADT-KomB (containing an N-terminal 3× Myc-Tag), pBADT-KomB^{m}(containing an N-terminal 3× Myc-Tag), pBADT-KomC (containing an N-terminal 3× Myc-Tag), pBADT-KomC^{m} (containing an N-terminal 3× Myc-Tag), pBADT-R1DNK (containing a C-terminal 3× FLAG-Tag), and pBADT-R1DNK^{m} (containing a C-terminal 3× FLAG-Tag) were constructed for analyzing the expression of mutant proteins. The coding sequence of T5dmp together with its native promoter (without the termination codon) was amplified from T5 phage genomic DNA using primers ZZF-14 and ZZF-15, and then inserted into the pBAD-Tag vector between the SphI and EcoRI sites, resulting in pBADT-T5Dmp. The plasmid encoding T5Dmp mutant (pBADT-T5Dmp^{D22A}) was constructed by the site-directed mutagenesis method using primers ZZF-44 and ZZF-45.

To analyze the effects of Dmp on the toxicity triggered by DNK and KomABC, a series of pETDuet-1-derived plasmids that express

Downloaded from https://www.science.org at Shanghai Normal University on February 22, 2025

DNKs or co-express DNKs and Dmps (wild type or mutant) were constructed. At first, we constructed pETDuet-araBAD by replacing a T7 promoter with the araBAD promoter from pBAD/His_A. Then, the coding sequences of different DNKs were inserted into pETDuet-araBAD and their expression is controlled by the araBAD promoter, generating the pETDuet-DNK plasmids. Next, the coding sequences of different Dmps together with the native promoter of T5Dmp were inserted into their respective pETDuet-DNK plasmids, generating the pETDuet-DNK_Dmp plasmids that co-express DNK and Dmp. The pETDuet-T5DNK-T5Dmp^{D22A} was constructed by the site-directed mutagenesis method using primers ZZF-44 and ZZF-45. The coding sequences of T5DNK and Dmp, Escherichia phage GreteKellenberger DNK and Dmp were amplified from the genomic DNA of the corresponding phages. The coding sequences of Vibrio phage VPG01 DNK and Dmp were synthesized by GENEWIZ (Suzhou, China).

To delete the *dmp* gene of T5, pCas13a-spT5Dmp that targets the *T5dmp* gene and pBAD-ΔT5Dmp that contains two homologous arms flanking the *T5dmp* gene were constructed. For the former, the spacer sequence targeting *T5dmp* was assembled by thermal annealing of two primers ZZF-58 and ZZF-59, and inserted into the linearized pBA559 plasmid (Addgene plasmid # 186235) using the restriction-ligation cloning method. For the latter, the two homologous arms were amplified from the T5 genomic DNA, assembled by overlapping PCR, and inserted into pBAD-Tag between the SphI and EcoRI sites. The plasmids pCas13a-spT5dnk, pCas13a-spR1DNK, pUC19-ΔT5 DNK, and pUC19-ΔR1DNK were constructed by the same method as described above for deleting the *dnk* genes of T5 and Rao1.

pQLink-R1DNK (containing an N-terminal Strep-Tag II), pQLink-T5Dmp (containing an N-terminal Strep-Tag II), pQLink-T5Dmp^{D22A} (containing an N-terminal Strep-Tag II), pCDF-KomC (containing an N-terminal 6×His tag), pCDF-KomA (containing an N-terminal 6×His tag), pQLink-NDK (containing an N-terminal 6×His tag), and pMAL-KomA (containing an N-terminal MBP tag) were constructed to express the recombinant proteins in *E. coli* BL21(DE3) for protein purification. The coding sequence of NDK was amplified from *E. coli* MG1655 genomic DNA, while the sequences of other genes were amplified from the previously constructed plasmids respectively. The sequences were inserted into the indicated vectors using ClonExpress assembly. To co-express R1DNK and KomA, the R1DNK expression cassette (containing the araBAD promoter) was amplified from the pBAD-R1DNK plasmid and then cloned into pRSFDuet-1, generating pRSF-R1DNK. Next, the coding sequence of KomA was amplified from pET28a-KomABC plasmid and inserted in the second multiple cloning site of pRSF-R1DNK, generating pRSF-R1DNK-KomA.

To co-express His-tagged KomC and KomB, the coding sequence of KomB was amplified from pET28a-KomABC plasmid using primers ZZF-24 and ZZF-25, and inserted into the second multiple cloning site of pCDF-KomC, generating pCDF-KomC-KomB. To co-express untagged KomC and KomB, PCR amplification was performed using pCDF-KomC-KomB as template and the primers ZZF-60 and ZZF-61. The resulting plasmid fragment was assembled using ClonExpress assembly (Vazyme, Nanjing, China), generating pCDF-KomC(tag-free)-KomB. The plasmids expressing the indicated mutated proteins were constructed by the site-directed mutagenesis method using the primers as listed in table S3.

Protein expression and purification

To obtain the recombinant proteins, the corresponding plasmids were transformed into *E. coli* BL21(DE3). The transformants were grown to an optical density (OD_{600}) of ~1.0 at 37°C in LB medium supplemented with appropriate antibiotics. Then, protein expression was induced with 0.4 mM isopropyl-β-D-thiogalactoside (IPTG) and/or 0.2% L-arabinose overnight at 16°C, except for T5Dmp and T5Dmp^{D22A}, the expression of which was induced with 0.4 mM IPTG at 37°C for only 5 min. The cells were collected by centrifugation at 7000 g for 10 min and the cell pellets were stored in -80°C freezer before protein purification.

To purify the His-tagged proteins (KomB-KomC complex, KomC, KomA, NDK), cell pellets were resuspended in lysis buffer (20 mM HEPES pH 7.5, 20 mM imidazole, 250 mM NaCl) and lysed by French press. The lysates were centrifuged at 13000 g for 1 hour at 4°C to remove cell debris, and the supernatants were then loaded onto a Ni-NTA column (Cytiva, 17531801) pre-equilibrated with lysis buffer. The column was washed with wash buffer (20 mM HEPES pH 7.5, 60 mM imidazole, 250 mM NaCl) and then the His-tagged proteins were eluted with elution buffer (20 mM HEPES pH 7.5, 300 mM imidazole, 250 mM NaCl). The eluted proteins were concentrated with Amicon centrifuge filters (Millipore, UFC8010) and then loaded onto a Superdex 200 Increase 10/300 GL column (Cytiva, 28990944) pre-equilibrated with buffer C (20 mM Tris-HCl, pH 7.5, 250 mM NaCl). The eluted proteins were concentrated again and stored at -80°C before use. The purity was analyzed by SDS-PAGE.

To purify the Strep-tagged protein (R1DNK, T5Dmp and T5Dmp^{D22A}), the cell pellet was resuspended in buffer C (20 mM Tris-HCl, pH 7.5, 250 mM NaCl) and lysed by French press. The lysate was centrifuged at 13000 g for 1 hour at 4°C to remove cell debris, and the supernatant was then loaded onto a Strep-Tactin®XT column (IBA Life Sciences, 2-5030-025) pre-equilibrated with buffer C. The column was washed with buffer C and then the Strep-tagged protein was eluted with buffer BXT (20 mM Tris-HCl, pH 7.5, 250 mM NaCl, 50 mM biotin). The eluted protein was concentrated with an Amicon centrifuge filter (Millipore, UFC8010) and then loaded onto a 5 ml HiTrap Desalting column (Cytiva, 29048684) pre-equilibrated with buffer C (20 mM Tris-HCl, pH 7.5, 250 mM NaCl). The eluted proteins were concentrated again and stored at -80°C before use. The purity was analyzed by SDS-PAGE.

Downloaded from https://www.science.org at Shanghai Normal University on February 22, 2025

Protein co-purification was performed to analyze the physical interaction between KomC and KomA, KomB or R1DNK. Specifically, *E. coli* BL21(DE3) cells carrying pRSF-R1DNK-KomA and pCDF-KomC^{m}-KomB (His-tagged KomC) were grown to an OD_{600} ~1.0 at 37°C in LB medium supplemented with appropriate antibiotics. Protein expression was induced with 0.4 mM IPTG and 0.2% L-arabinose at 16°C for 16 hours. The cell lysate preparation and Ni-NTA affinity chromatography were carried out using the same method for His-tagged proteins as described above. In addition, protein expression and purification were also performed with *E. coli* BL21(DE3) cells carrying pRSF-R1DNK-KomA and pCDF-KomC^{m} (tag-free)-KomB (untagged KomC). The fractions from the Ni-NTA affinity chromatography were subjected to mass spectrometry.

To obtain the putative second messenger bound by the KomB-KomC complex, *E. coli* BL21(DE3) cells co-expressing R1DNK or its mutant and KomABC or the mutated systems were used to purify the different versions of KomBC complexes, i.e., KomBC-1 (pCDF-KomC-KomB and pRSF-R1DNK^{K15A}-KomA), KomBC-2 (pCDF-KomC-KomB and pRSF-R1DNK-KomA^{m}), H^{m}S (pCDF-KomC-KomB^{m} and pRSF-R1DNK-KomA) and KomBC^{m} (pCDF-KomC^{m}-KomB and pRSF-R1DNK-KomA) (Fig. 3C). Culture growth, protein expression induction and Ni-NTA affinity chromatography were carried out with the same method as described above, except the column was washed with lysis buffer instead of the wash buffer. The elution fractions were concentrated to 1 ml using Amicon centrifuge filters (Millipore, UFC8010) and analyzed by SDS-PAGE (fig. S11A). The concentrated protein samples were denatured to release the bound molecules.

Phage propagation and plaque assay

Phages were propagated using *E. coli* MG1655 as the host. Overnight cultures of *E. coli* MG1655 were diluted 1:100 in MMB medium (LB supplemented with 0.1 mM $MnCl_2$, 5 mM $MgCl_2$) and grown to an OD_{600} of ~0.3 at 37°C. Then, 1 ml of the culture was infected with phages of interest at a multiplicity of infection (MOI) of 0.01 and further grown for 4 hours. The cultures were centrifuged at 5000 g for 10 min and the supernatants were filtered through 0.22 μm membrane filters (Millipore, SLGPM33RS) to remove the cells. The resulting phage shocks were stored at 4°C.

A double agar overlay assay was used to determine phage titer. In brief, phage stocks were 10-fold serially diluted in SM buffer (50 mM Tris-HCl, pH 7.5, 100 mM NaCl, 8 mM $MgSO_4$). Three μl of the serial dilutions (from 10^{-3} to 10^{-8}) were mixed with 300 μl of the overnight cultures of the *E. coli* host as indicated before and 4 ml melted MMB + 0.5% agar, and then poured onto MMB + 1.5% agar plates. Plates were incubated at 37°C overnight. Plaque-forming units (PFUs) were determined by counting the derived plaques.

For plaque assays, *E. coli* host cells expressing an empty vector (pET28a) or wild type or mutated KomABC systems were grown in MMB medium supplemented with kanamycin (50 μg/ml) at 37°C overnight. Then, 300 μl of the cultures were mixed with 8 ml melted MMB + 0.5% agar + kanamycin (50 μg/ml) and poured onto MMB + 1.5% agar + kanamycin (50 μg/ml) plates. Meanwhile, phages of interest were 10-fold serially diluted in SM buffer and 3 μl of the 10-fold serial dilutions were spotted on the bacterial overlay. The plates were incubated at 37°C for 8 hours before images of the plates were captured.

To analyze the function of T5Dmp, The *E. coli* MG1655 cells carrying pCDFduet empty vector or pCDF-KomABC were further transformed with an empty vector (pBAD/His_A) or pBAD-T5Dmp or pBAD-T5Dmp^{D22A}. The transformants were grown in MMB medium supplemented with ampicillin (100 μg/ml) and kanamycin (50 μg/ml) at 37°C overnight. Then, 300 μl of cultures were mixed with 8 ml melted MMB + 0.5% agar + ampicillin (100 μg/ml) and kanamycin (50 μg/ml) and poured onto MMB + 1.5% agar + ampicillin (100 μg/ml) and kanamycin (50 μg/ml) plates. Meanwhile, phage Rao1 was 10-fold serially diluted in SM buffer and 3 μl of the 10-fold serial dilutions were spotted on the bacterial overlay. The plates were incubated at 37°C for 8 hours before images of the plates were captured.

Phage-infection dynamics in liquid medium

Overnight cultures of *E. coli* MG1655 containing an empty vector (pET28a) or pET28a-KomABC were diluted 1:100 in MMB medium supplemented with kanamycin (50 mg/ml) and grown to OD_{600}~0.2 at 37°C. Then, 180 μl of the cultures were transferred into wells of a 96-well plate, and 20 μl of the diluted phages were added into the cultures for a final MOI of 0.3 or 3. The uninfected culture (MOI = 0) was supplemented with 20 μl SM buffer. OD_{600} was measured every 5 min with shaking at 200 rpm at 37°C in a FLUOstar OMEGA (BMG Labtech, Germany).

Toxicity assays on solid medium

To analyze the toxicity triggered by the co-expression of the KomABC system and R1DNK, the colony-forming units (CFUs) per ml of the cells co-expressing KomABC and R1DNK were determined. Specifically, *E. coli* MG1655 cells containing pCDFduet-derived plasmids (pCDFduet empty vector or pCDF-KomABC) and pBAD/His_A -derived plasmids (pBAD/His_A empty vector, pBAD-R1DNK or pBAD-R1DNK^{K15A}) were grown overnight at 37°C in MMB supplemented with streptomycin (50 μg/ml) and ampicillin (100 μg/ml). The overnight cultures were then diluted 1:100 in MMB supplemented with appropriate antibiotics and grown to OD_{600}~0.8 at 37°C. The cultures were subsequently 10-fold serially diluted in MMB. Five μl of 10-fold serial dilutions (from 10^{-1}-10^{-6}) were spotted on MMB plates supplemented with appropriate antibiotics and 1% glucose or 0.05% L-arabinose. The plates were incubated at 37°C overnight before images of the plates were captured. The toxicity triggered by the co-expression of the KomABC system and DNKs from other phages was analyzed in a similar

Downloaded from https://www.science.org at Shanghai Normal University on February 22, 2025

procedure.

To analyze the effects of T5Dmp on the toxicity triggered by the co-expression of the KomABC system and T5DNK, The CFUs per ml of *E. coli* MG1655 cells containing pCDFduet-derived plasmids (pCDFduet empty vector or pCDFduet-KomABC) and pETduet-derived plasmids (pETduet-T5DNK, pETduet-T5DNK-T5Dmp or pETduet-T5DNK-T5Dmp^{D22A}) were determined as described above. The effects of Dmps from other phages on the DNK-triggered toxicity were analyzed in the same protocol.

Toxicity assays in liquid medium

Single colonies of *E. coli* MG1655 harboring pCDFduet empty vector and pBAD-R1DNK, pCDF-KomABC and pBAD-R1DNK, or pCDF-KomABC and pBAD-R1DNK^{K15A} were grown at 37°C overnight in MMB supplemented with streptomycin (50 μg/ml), ampicillin (100 μg/ml). Overnight cultures were diluted 1:100 in MMB supplemented with streptomycin (50 μg/ml), ampicillin (100 μg/ml) and 0.2% arabinose, and 200 μl of diluted cultures were transferred into wells of a 96-well plate. The plate was incubated at 37°C with shaking at 200 rpm in a FLUOstar OMEGA (BMG Labtech, Germany) and OD_{600} was measured every 5 min.

Isolation of phage escape mutants

The plaque assay was used to isolate mutant phages that evaded the defense of the KomABC system, as described previously (*25*). Briefly, 300 μl of overnight culture of *E.coli* MG1655 harboring pET28a-KomABC plasmid was mixed with 8 ml melted MMB + 0.5% agar + kanamycin (50 μg/ml) and poured onto MMB + 1.5% agar + kanamycin (50 μg/ml) plates. Three microliters of the 10-fold serially diluted Rao1 phage stock was spotted on the bacterial overlay, and then the plates were incubated at 37°C overnight. Single plaques were isolated and propagated using *E. coli* MG1655 at 37°C for 4 hours. The cultures were centrifuged for 10 min at 5000 g and the supernatants were filtered through 0.22 μm membrane filters to remove the cells. The resulting phage solution of Rao1 phage mutants was 10-fold serially diluted in SM buffer. Three microliters of the 10-fold serial dilutions of wild type Rao1 and Rao1 mutants were spotted on the bacterial overlay of *E. coli* MG1655 containing pET28a or pET28a-KomABC. The plates were incubated at 37°C for 8 hours and then images of the plates were captured.

Extraction and sequencing of phage DNA

To extract phage DNA, 500 μl of phage stocks were treated with DNase I (5 U/ml) (Thermo Fisher Scientific, EN0521) and RNase A (50 μg/ml) (Thermo Fisher Scientific, R1253) at 37°C for 1 hour to degrade bacterial DNA and RNA. The phage stocks were then incubated with proteinase K (0.5 mg/ml) (Thermo Fisher Scientific, EO0491) at 37°C for 1 hour, followed by supplementation of 500 μl of phenol/chloroform/isoamyl alcohol (pH 8.0, 25:24:1). The samples were then vortexed briefly and centrifuged at 13000 g at 4°C for 15 min. The upper water phase (about 400 μl) was transferred into a 1.5 ml tube and mixed with 400 μl of chloroform. The mixtures were then vortexed briefly and centrifuged at 13000 g for 15 min at 4°C. The upper water phase (about 400 μl) was isolated to a 1.5 ml tube and mixed with 40 μl 3 M NaAc (pH 5.2) and 400 μl isopropanol. The mixtures were then vortexed briefly and incubated at -20°C for 4 hours. After incubated, the mixtures were centrifuged at 13000 g at 4°C for 15 min and the supernatant was discarded. The pellets were washed with 75% ethanol (pre-cooled to -20°C) and dried for 10 min. The pellets were resuspended in 30 μl DEPC H_2O.

Libraries preparation and sequencing were performed by Novogene (Beijing, China). Briefly, sequencing libraries were prepared using Annoroad® Universal DNA Fragmentase kit V2.0 (AN200101-L) and Annoroad® Universal DNA Library Prep Kit V2.0 (AN200101-L) according to the instructions of the manufacturer. Libraries were sequenced on Novaseq 6000 S4 platform with PE150 strategy.

The sequencing data with the host genome removed were aligned to phages using bwa (v0.7.17-r1188) (*54*). Duplicate reads in the bam files were removed using picard MarkDuplicates (v3.1.1). Variant detection was conducted using bcftools (v1.18) (*55*), starting with variant calling using mpileup (option "–output-type u") and call (option "–multiallelic-caller–variants-only–output-type v"), followed by filtering with filter (option "-g 3 -G 10 -e 'QUAL<40 || DP<10' "). Finally, SNPs (single nucleotide polymorphisms) and indels (insertion-deletions) were detected with bcftools view. The annotation of variant results was performed using the annovar software (option "-geneanno–neargene 100").

Quantification of relative cellular NAD$^+$ levels

The relative content of cellular NAD^+ was measured by the MTT (Methyl Thiazolyl Tetrazolium) assay as described previously (*30*). Specifically, *E. coli* MG1655 cells expressing wild-type or mutant KomABC and wild-type or mutant R1DNK were grown at 37°C overnight in MMB supplemented with streptomycin (50 μg/ml), ampicillin (100 μg/ml). Overnight cultures were diluted 1:100 in MMB supplemented with appropriate antibiotics and grown at 37°C until OD_{600} reached 0.2. Then, expression of R1DNK or its mutant were induced with 0.2% L-arabinose for 30 min at 37°C. 4 ml of cultures (OD_{600} ~0.3) were collected by centrifugation at 4000 g for 5 min. The supernatant was removed and the cell pellets were washed with 600 μl PBS buffer (pH 7.4). The cells were collected again by centrifugation at 4000 g for 5 min again. The cellular NAD^+ content was measured using the Coenzyme I NAD(H) content detection kit (Solarbio, BC0315) according to the instructions of the manufacturer. The optical density at 570 nm of each sample was measured to reflect the NAD^+ content in the sample. The relative NAD^+ content of each sample was calculated using the following equation:

Relative NAD^+ content = (OD^{sample} - $OD^{sample_control}$) / (OD^{EV}-

Downloaded from https://www.science.org at Shanghai Normal University on February 22, 2025

$OD^{EV_control}$)

Control, the NAD^+ in the sample was neutralized before supplementation of MTT; EV, the cells containing empty vectors. All samples were performed in three biological replicates.

Pull-down assay

To analyze the physical interaction between R1DNK and KomA, KomB-KomC complex (KomBC), the bait protein (20 μg Strep-R1DNK) was incubated with 20 μg purified KomA or 20 μg purified KomBC, or a mixture of them in 200 μl buffer C at 4°C for 30 min. Then, the protein mixtures were incubated with pre-equilibrated 40 μl Strep-Tactin resin (IBA Life Sciences, 2-5030-025) at 4°C for 30 min. The resins were washed with 500 μl buffer C for five times. The bound protein was eluted in 100 μl BXT buffer and analyzed by SDS-PAGE.

To analyze the physical interaction between KomA and KomBC, the bait protein (20 μg MBP or MBP-KomA) was incubated with 20 μg purified KomBC in 200 μl buffer C at 4°C for 30 min. Then, the protein mixtures were incubated with pre-equilibrated 80 μl Dextrin Beads (Smart-Life sciences, SA026005) at 4°C for 30 min. The beads were washed with 500 μl buffer C for three times. The bound protein was eluted in 100 μl buffer C supplemented with 10 mM maltose and analyzed by SDS-PAGE.

Western blot

For protein mutant expression analysis, *E. coli* MG1655 strain harboring the corresponding plasmid was grown to an OD_{600} of ~0.3 at 37°C in MMB medium supplemented with appropriate antibiotics and 0.2% arabinose. 5 ml of cultures were collected and resuspended in 600 μl buffer C. Cells were disrupted by ultrasonication, followed by centrifugation at 13000 g at 4°C for 15 min to remove the debris. The proteins were separated by SDS-PAGE and then transferred to PVDF membranes (Bio-Rad, Hercules, CA, USA). Membranes were blocked in TBST buffer (50 mM Tris, 100 mM Nacl, 0.05% Tween 40, pH 8.0) supplemented with 6% milk at 25°C for 2 hours, followed by incubation with anti-FLAG (Abbkine, ABT2011,1:4000) or anti-Myc (Abbkine, ABT2061, 1:5000) primary antibodies diluted in TBST buffer supplemented with 6% milk overnight at 4°C. Membranes were washed three times with TBST buffer, followed by incubation with secondary antibodies (Abbkine, A21020, 1:10000) at 25°C for 2 hours and visualized using Tanon 5200 (Tanon, Shanghai, China).

Deoxynucleotide monophosphate kinase assay

For deoxynucleotide monophosphate kinase assay, a 50-μl reaction mixture containing 50 mM HEPES pH 7.5, 50 mM KCl, 10 mM $MgCl_2$, 1 mM ATP, 1 mM TCEP, 1 mM nucleotide substrate (dAMP, dGMP, dCMP, dTMP, dIMP, AMP, or IMP) and 1 μM R1DNK was incubated at 37°C for 1 hour. Then, the mixture was heated to 90°C for 5 min to stop the reactions, followed by centrifugation at 13000 g at 4°C for 15 min to remove the precipitated protein. The supernatant was supplemented with 750 μl of buffer A (5 mM Tris-HCl pH 8.0) and loaded onto a MonoQ 5/50 column (GE Healthcare, USA). The bound nucleotides were eluted using a linear gradient from 0 to 0.4 M NaCl over 25 ml.

The nucleotides used for all experiments were purchased from the following companies. dGMP (A600363), dCMP (A600361), dTMP (A600367), dUTP (B600006) and 2'-deoxyadenosine (A620043) were purchased from Sangon Biotech. dAMP (S18087), dIMP (S18105), AMP (B24464), IMP (S18082), ADP (B25056), dATP (S18090), dCDP (S18096), dTDP (S18109), inosine (B20582) and ITP (S18084) were purchased from Yuanye. ATP (R0441) and dITP (R1191) were purchased from Thermo Fisher Scientific. dADP (GC11854) was purchased from GlpBio. 2'-deoxyinosine (532038) was purchased from J&K Scientific. dGDP (D119530) was purchased from Aladdin.

Adenosine deaminase assay

To perform the adenosine deamination assay, a 50-μl reaction mixture containing 50 mM HEPES pH 7.5, 50 mM KCl, 1 mM TCEP, 1 mM substrate (dATP, dADP, dAMP, ATP, ADP or AMP) and 5 μM KomA was incubated at 37°C for 1 hour. After heated to 90°C for 5 min to stop the reactions, the reaction mixtures were supplemented with 1.5 μl FastAP Thermosensitive Alkaline Phosphatase (Thermo Fisher Scientific, EF0654) and incubated at 37°C for 15 min. Then, the mixtures were supplemented with 350 μl MilliQ H_2O and centrifuged at 13000 g for 10 min to remove precipitated protein. The supernatant was passed through 0.2 μm Filters for Ultrahigh-performance liquid chromatography (UHPLC) analysis.

The HPLC analysis was performed using a Nexera UHPLC System (Shimadzu, Japan) with a C18 column (Kinetex 3×100 mm, particle size 2.6 μm) for both the reaction products and the standards. The column was warmed to 35°C and the flow rate was 0.3 ml/min. Threemicroliters of each sample was loaded. Gradient elution was performed with solvent A (5 mM ammonium acetate) and solvent B (100% acetonitrile). The gradient elution proceeded as follows: 0 to 2 min, 5% B; 2 to 7 min, 5 to 10% B; 7 to 10 min, 10 to 95% B; 10 to 18 min, 5% B.

To analyze the effects of divalent metal ions on the adenosine deamination activity of KomA, the assay was performed with dAMP as substrate in the presence of 0.5 mM different divalent metal ions Mg^{2+}, Ni^{2+}, Cu^{2+}, Zn^{2+}, Mn^{2+}) or 0.5 mM EDTA.

εNAD-based NADase assay

To analyze the NADase activity of KomB-KomC complex (KomBC) and the mutated complexes, a 50-μl reaction mixture containing 50 mM HEPES pH 7.5, 50 mM KCl, 1 mM TCEP, 50 μM nicotinamide 1, N^6-ethenoadenine dinucleotide (εNAD, Sigma, N2630), and the indicated enzymes, nucleotides, metal ions and/or reaction products was prepared in black 96-well half area plates (Greiner Bio-One, 675076). Then, the plates were

Downloaded from https://www.science.org at Shanghai Normal University on February 22, 2025

immediately incubated in a Spark multimode microplate reader (Tecan, Switzerland) at 37°C and fluorescence intensity was measured every 30 s over 30 min at 300 nm excitation wavelength and 410 nm emission wavelength. The concentrations of the KomBC complex in the reaction were calculated based on the estimation that the ratio of KomB and KomC is 1:1 according to the band density in SDS-PAGE gel and the protein mass spectrometry analysis.

To analyze the NADase activity of standalone KomC and KomBC complex (Fig. 2E), the reaction mixtures contained 0.1 mM $ZnSO_4$ and 0.8 μM KomC or KomBC.

To analyze the effects of divalent metal ions on the NADase activity (fig. S10A), the reaction mixtures contained 0.8 μM KomBC and 1 mM divalent metal ions (Mg^{2+}, Ni^{2+}, Cu^{2+}, Zn^{2+}, Mn^{2+}) or 1 mM EDTA. Except for the metal dependency assay, all other reactions contained 0.1 mM $ZnSO_4$.

To analyze whether the NADase activity is activated by nucleotides (Fig. 3A), the reaction mixtures contained 50 nM KomBC and 100 nM different nucleotides (dNTP, NTP, dITP, dUTP, ITP, IDP, IMP). The effects of dITP and IDP on the NADase activity were further analyzed with a gradient of dITP (0, 0.1 nM, 1 nM, 10 nM, 100 nM) and IDP (0, 10 nM, 100 nM, 1000 nM) (fig. S10C-D).

To analyze the NADase activity of mutated KomBC complexes ($KomB^m$-KomC and KomB-$KomC^m$), the concentrations of wild type KomBC, $KomB^m$-KomC or KomB-$KomC^m$ in the reaction mixtures were 0.6 μM (Fig. 2G). To analyze the activation of mutated KomBC complexes by dITP, the concentrations of wild type and mutated complexes were 50 nM and 1 nM dITP was further supplemented (Fig. 3B).

To analyze whether the reaction products of KomA and *E. coli* NDK with dADP as substrate and ATP as phosphate group donor activate the NADase activity of KomBC, the adenosine deamination reaction mixtures containing 50 mM HEPES pH 7.5, 50 mM KCl, 1 mM TCEP, KomA (0 or 5 μM), 100 nM dADP, were incubated at 37°C for 60 min, and further supplemented with 100 μM $ZnSO_4$,10 mM $MgCl_2$, NDK (0 and 1.6 μM) and 1 μM ATP, followed by incubation at 37°C for 15 min. Then, the mixtures were heated at 90°C for 5 min to stop the reactions. After the precipitated protein was removed by centrifugation at 13000 g at 4°C for 15 min, the reaction products were tested for its capability of activating the NADase activity of KomBC in reaction mixtures containing 50 nM KomBC (Fig. 4F).

To analyze whether the reaction products of R1DNK and *E. coli* NDK with dIMP as substrate and ATP as phosphate group donor activate the NADase activity of KomBC, the reaction mixtures containing 50 mM HEPES pH 7.5, 50 mM KCl, 1 mM TCEP, 10 mM $MgCl_2$, R1DNK (0 or 2.4 μM), 1 mM ATP, 1 μM dIMP, were incubated at 37°C for 60 min, and further supplemented with 100 μM $ZnSO_4$ and NDK (0 or 1.6 μM), followed by incubation at 37°C for 15 min. Then, the mixtures were heated at 90°C for 5 min to stop the reactions. After the precipitated protein was removed by centrifugation at 13000 g at 4°C for 15 min, the reaction products were tested for its capability of activating the NADase activity of KomBC in reaction mixtures containing 50 nM KomBC (Fig. 4G).

To analyze whether the released molecules from the denatured protein samples (KomBC-1, KomBC-2, $KomB^mC$ and $KomBC^m$) activate the NADase activity of KomBC, 1 ml of KomBC-1, KomBC-2, $KomB^mC$ and $KomBC^m$ were heated to 90°C for 10 min and then centrifuged at 13000 g at 4°C for 15 min to remove the precipitated protein. Then, NADase assay were performed in a 50-μl reaction mixture containing 50 nM KomBC and 0.01% (v/v) of the heated samples of KomBC-1, KomBC-2, $KomB^mC$ and $KomBC^m$ (fig. S11C).

UHPLC analysis of the NADase reaction products

To analyze the products of NADase reactions, a 50-μl reaction mixture containing 50 mM HEPES pH 7.5, 50 mM KCl, 1 mM TCEP, 1 mM NAD^+ (Yuanye, B27081), 100 μM $ZnSO_4$, 100 nM KomBC and dITP (0 or 1 nM) was incubated at 37°C for 30 min. The reaction mixtures were heated to 90°C for 5 min and then 450 μl MilliQ H_2O was supplemented. The mixtures were then centrifuged at 13000 g for 10 min to remove precipitated protein and the supernatants was passed through 0.2 μm Filters for UHPLC analysis.

The reaction products and standards (NAD^+(Yuanye, B27081), ADPR (MCE, HY-100973A), NAM (Yuanye, B21424)) were analyzed using a Nexera UHPLC System (Shimadzu, Japan) with a C18 column (Kinetex, 3×100 mm, particle size 2.6 μm). The column was warmed to 30°C and the flow rate was 0.3 ml/min. Three μl of each sample was loaded. Gradient elution was performed with solvent A (0.1% (v/v) formic acid and 5 mM ammonium formate in water) and solvent B (0.1% (v/v) formic acid and 5mM ammonium formate in methanol). The gradient elution proceeded as follows: 0 to 5 min, 0% B; 5 to 7 min, 0% to 95% B; 7 to 7.5 min, 95% B; 7.5 to 8 min, 95% to 0% B, 8 to 21 min 0% B.

Phage T5 genome editing

T5 *dmp* gene was knocked out following a published method (*28*) with modifications. Briefly, *E. coli* MG1655 cells harboring pBAD-ΔT5dmp plasmid (a homologous recombination plasmid) were grown in MMB medium with ampicillin (100 μg/ml) overnight at 37°C. The overnight culture was diluted in MMB medium with ampicillin (100 μg/ml) to OD_{600}~0.2. Then, 500 μl of the culture was infected with wild type T5 phage at an MOI of 0.01 and grown at 37°C for 4 hours. The culture was centrifuged for 10 min at 5000 g and the supernatants were filtered through 0.22 μm membrane filters to remove the cells. This resulted in a mixture of wild type T5 phage and homologous recombination-edited T5 phage. The phage titer of the mixture was determined using the double agar overlay assay as described above.

Then, *E. coli* MG1655 cells harboring the pCas13a-spT5dmp plasmid, which carried a spacer targeting *dmp*, were grown in MMB medium containing chloramphenicol (25 μg/ml) overnight at 37°C. The overnight culture was diluted in MMB medium

Downloaded from https://www.science.org at Shanghai Normal University on February 22, 2025

supplemented with chloramphenicol (25 μg/ml) and 80 ng/ml aTc to OD_{600}~0.2. Then, 500 μl of the culture was infected with the mixture of wild type T5 phage and homologous recombination-edited T5 phage at an MOI of 0.01 and grown at 37°C for 4 hours. The culture was centrifuged for 10 min at 5000 g and the supernatant was filtered through 0.22 μm membrane filters to remove the cells. The resulting phage mixture was used to infect the cells harboring the pCas13a-spT5dmp plasmid again to enrich the homologous recombination-edited T5 phage.

To select the homologous recombination-edited T5 phage, the mixture of wild type T5 phage and homologous recombination-edited T5 phage were 10-fold serially diluted in SM buffer and 3 μl of 10-fold serial dilutions were spotted on the bacterial overlay prepared with *E. coli* MG1655 cells harboring pCas13a-spT5dmp. Then, the plates were incubated at 37°C for 8 hours and single plaques were analyzed with PCR using the primer set ZZF-14 and ZZF-15. The propagation of T5 mutants was performed with *E. coli* MG1655 cells as the host as described above.

A similar method was used to knockout T5DNK and R1DNK.

Fitness assay of mutant phages

Phages competition assays were performed following a published method (*25*) with minor modifications. Each pair of mutant and wild-type phages was mixed at an approximate ratio of 1:1 as the ancestor of phage mixture (cycle 0). The cultures of *E. coli* MG1655 were grown to an OD_{600} of 0.2 at 37°C shaking at 180 rmp. Then the cultures were infected with the phage mixture at a final MOI ~ 0.01, and incubated for 4 hours at 37°C shaking at 180 rmp. the culture was centrifuged at 8000 g for 5 min to remove cells and debris, and the phage titer in the supernatant was assessed using the same method as described above. Subsequently, a fresh culture of *E. coli* MG1655 were infected with the resulting supernatant at a final MOI ~ 0.01 (cycle 2). These cycles (1, 2, and 3) were performed three times, and these resulting phage mixtures were sampled for phage DNA extraction and sequencing as described above. For the origin of the phage mixtures (cycle 0), 500 μl of the phage mixture was extracted for sequencing.

The sequenced reads were aligned with the mutant phage genome sequence, and the ratio of each mutant reads to wild-type reads was calculated based on the reads aligned at the expected mutation position. The sequencing reads were aligned to phages genome using bwa (v0.7.17-r1188).

dITP pyrophosphatase assay of KomBC

To analyze whether KomBC has dITP pyrophosphatase activity, a-50 μl reaction mixture containing 50 mM HEPES pH 7.5, 50 mM KCl, 1 mM TCEP, 100 μM $ZnSO_4$, KomBC (0 or 3.2 μM) and 1 mM dITP was prepared and incubated at 37°C for 60 min. The reaction mixtures were heated to 90°C for 5 min to stop the reaction, and the reaction products were analyzed using ion-exchange chromatography as described in "Deoxynucleotide monophosphate kinase assay."

Deoxynucleoside 5'-phosphatase assays

Deoxynucleoside 5'-phosphatase activity of T5Dmp was analyzed following a published method (*40*) with modifications. Briefly, the reactions were prepared in a 50 μl reaction mixture containing 50 mM Tris-HCl pH 7.5, 50 mM NaCl, 0.1 mg/ml BSA, 4 mM DTT, 30 mM $MgCl_2$, 0.5 μM T5Dmp protein (wild type or mutant) and 1 mM different deoxynucleotide substrates (dNMP, dITP, dATP, dADP, dIMP) at 30°C for 30 min. The reaction mixtures were heated to 90°C for 5 min to end reactions. The reaction products were analyzed using UHPLC as described in the Deaminase assay.

Protein identification by mass spectrometry (MS)

Protein MS was performed by Novogene (Beijing, China). To identify the purified protein bands, i.e., the putative KomB protein purified from cells co-expressing His-KomC and KomB, the protein samples were separated by 10% SDS-PAGE and visualized with Coomassie brilliant blue. The protein band indicated in Fig. 2C was excised and sent for MS analysis by Novogene (Beijing, China). Briefly, the proteins in gel were digested by trypsin with a standard protocol of Novogene, and the digested peptides were analyzed by an EASY-nLC 1200 UHPLC (Thermo Fisher) coupled with an Q Exactive™ HF-X mass spectrometer (Thermo Fisher) using a standard LC-MS/MS method.

MS was also used to identify the proteins co-purified with His-tagged KomC or untagged KomC (Fig. 2B). The proteins were also digested by trypsin. The digested peptides were desalted with a C18 desalting column and lyophilized. Then, the digested peptides were analyzed by a nanoElute UHPLC (Bruker) coupled with a tims TOF pro2 (Bruker) using a standard LC-MS/MS method.

Peptide spectrum matches (PSMs) were performed in Proteome Discoverer (PD, Thermo) or MaxQuant (Bruker, Tims) against *Escherichia coli* (strains B / BL21-DE3) proteome database (Uniprot, UP000009074) and the 4 additional proteins (KomA, KomB, KomC, R1DNK) with their amino acid sequences. The search results were filtered with PD/MaxQuant software to improve the quality of the search results. PSMs with a confidence level of 99% or more were considered as credible PSMs. The identified proteins contain at least 1 unique peptide. False discovery rate (FDR) validation was performed to remove the peptides and proteins with FDR greater than 1%. To determine the significance of the differences, the Significance A test was performed on the relative quantitative values of each protein in the two comparison sample pairs (*56*), and the corresponding P-value was calculated. Proteins with significant quantitative differences between the His-tagged KomC group and the untagged KomC group ($p < 0.1$, $|\log_2 FC| > 1$ ($FC > 2$ or $FC < 0.5$ [fold change, FC]) were defined as differentially expressed proteins (DEP).

Downloaded from https://www.science.org at Shanghai Normal University on February 22, 2025

LC-MS/MS

LC-MS/MS was used to identify the released molecules from the denatured protein samples (KomBC-1, KomBC-2, KomB^{m}C and KomBC^m) and the reaction products of KomA and *E. coli* NDK with dADP and ATP. For the former, 1 ml of KomBC-1, KomBC-2, KomB^{m}C and KomBC^m were heated to 90°C for 10 min and then centrifuged at 13000 g at 4°C for 15 min to remove precipitated protein. The supernatant was filtered through 0.22 μm membrane filters for LC-MS/MS analysis. For the latter, the reaction of KomA and *E. coli* NDK with dADP and ATP was performed as described in the εNAD-based NADase assay, except that the 50-μl reaction mixtures contained 1 mM dADP, 0 or 20 μM KomA, 2 mM ATP and 0 or 4 μM NDK. Then the mixtures were heated to 90°C for 5 min to stop the reaction, and supplemented with 150 μl MilliQ H_2O. The mixtures were then centrifuged at 13000 g for 10 min to remove precipitated protein and the supernatants was passed through 0.2 μm Filters for LC-MS/MS analysis. The reaction of R1DNK with dIMP and ATP was performed as described in the εNAD-based NADase assay, except that the 100-μl reaction mixtures contained 1 mM dIMP, 5 μM R1DNK, 3 mM ATP. Then the mixtures were heated to 90°C for 5 min to stop the reaction. The mixtures were then centrifuged at 13000 g for 10 min to remove precipitated protein and the supernatants were passed through 0.2 μm filters for LC-MS/MS analysis.

The LC–MS/MS analysis was performed using an UltiMate 3000 UHPLC System coupled to the Q Exactive Plus Orbitrap high-resolution mass spectrometry (Thermo Fisher Scientific). The UHPLC was performed using an InfinityLab PoroShell 120 HILIC-Z PEEK lined column (Agilent Technologies, 2.1 × 100 mm, particle size 2.7 μm). The column was warmed to 30°C and the flow rate was 0.3 ml/min. Three μl of each sample was loaded onto the column. Gradient elution was performed with solvent A (10 mM ammonium acetate at pH 9 in ultra-pure water) and solvent B (10 mM ammonium acetate at pH 9 in 90% acetonitrile and 10% ultra-pure water). The gradient elution proceeded as follows: 0 to 12 min, 90% to 50% B; 12 to 13 min, 50% B; 13 to 13.1 min, 50% to 90% B; 13.1 to 26 min, 90% B.

MS/MS analysis was performed in negative ionization mode from 100 to 1200 m/z at a mass resolution of 70,000. Synthetic dITP (Thermo Fisher Scientific, R1191) was also run to identify the dITP standard peaks. The reaction product of KomA and dADP was used as dIDP standard. MS/MS spectra collection was performed at a resolution of 17,500. Data analysis was performed using Xcalibur Qual Browser (Thermo Fisher Scientific).

Quantification of nucleotides by UHPLC-MS/MS

To analyze the nucleotides in cells infected by phages, overnight cultures of *E. coli* MG1655 were diluted 1:100 in 200 ml MMB medium and grown to an OD_{600} of 0.3 at 37°C. 45 ml of cultures were sampled (Unifected), and then the rest cultures were infected with wild-type phage or mutants at a final MOI of 3. Subsequently, 45 ml of infected cultures were taken at indicated times (5 min, 10 min, and 15 min for T5 or 8 min, 16 min, and 24 min for Rao1) and centrifuged (8000 g, 4°C) for 5 min to remove supernatants.

To analyze the nucleotides in cells expressing Kongming and R1DNK, the mutated system (KomABC^m) was expressed from its native promoter, while R1DNK was expressed from an arabinose promoter. The cells were collected after the expression of R1DNK was induced for 1 hour.

The pellets were resuspended in 700 μl of cold extraction solvent (acetonitrile, methanol, water, formic acid = 2:2:1:0.02, v/v/v/v) and lysed by ultrasonication for 1 min, followed by centrifugation at 13000 g at 4°C for 15 min to remove the debris. The supernatants were dried by lyophilization using a freeze dryer (Lichen LC-10N-50C), then resuspended in 100 μl water and analyzed by UHPLC-MS/MS. For analyses of the nucleotides in cells expressing R1DNK, the method was similar to that described above, except that MMB medium was supplemented with 0.2% arabinose and corresponding antibiotic and samples were taken at 60 min post-induction.

Quantification of nucleotides were performed using an UltiMate 3000 UHPLC System coupled to a TSQ Plus triple quadrupole mass spectrometer (Thermo Fisher Scientific). The UHPLC was performed as described in "Liquid chromatography-tandem mass spectrometry." The analyses were performed in positive ion modes (dATP, dADP, dAMP) or negative ionization mode (dIMP, dIDP, dITP). Nucleotides were detected and quantified using multiple reaction monitoring (MRM).

A standard curve of dITP was constructed within the concentration range from 5 μM to 60 μM for quantification of the released dITP from the denatured protein samples. Metabolites (dATP, dADP, dAMP, dIMP, dIDP, and dITP) were quantified using product ion area. Data analysis was performed using Xcalibur Qual Browser (Thermo Fisher Scientific).

Identification of DNK/Dmp homologs

Phage DNK and Dmp homologs were identified in the INPHARED database (release 1Mar2024) (*57*). The protein set used to construct HMM models for DNK and Dmp were identified using HMMER v3.4's jackhmmer (*58*) with an E-value of 1e-3, employing T5 DNK (YP_006871.1) and Dmp (YP_006829.1) sequences as queries against our phage collection database. HMM profiles were generated using HMMbuild after removal of redundant sequences by CD-HIT v4.8.1 (*59*) with sequence identity threshold 100% and length difference cutoff 100%. DNK and Dmp homologs were identified using the generated HMM profiles as query against INPAHARED database of RefSeq complete phage genomes with an E-value threshold of 1e-3.

Phylogenetic tree construction

To construct phage phylogenetic tree, the phages used in this

Downloaded from https://www.science.org at Shanghai Normal University on February 22, 2025

study were clustered using Genome-BLAST Distance Phylogeny (GBDP) method with the D0 formula for nucleotides in VICTOR (*60*). Taxonomy information was retrieved from NCBI database or BASEL phage collection (*53*).

KomB domain-containing proteins were retrieved using HMMER v3.4's hmmsearch with the Pfam HMM profile PF01725 as the query against the RefSeq non-redundant protein database. Proteins with sequences longer than 100 amino acids were clustered using MMseqs2 easy-cluster (*61*). Representative sequences were aligned using hmmalign with the '-trim' flag, and a phylogenetic tree was constructed using FastTree v2.1.11 (*62*) with gamma-distributed site rates and the WAG evolutionary model.

For other phylogenetic trees, sequences were first aligned with MAFFT v7.525 FFT-NS-1000 (*63*) and trimmed using trimAl v1.5.0 (*64*) to remove any column in the alignment that has more than 30% gaps. Phylogenetic tree construction was performed using FastTree with gamma-distributed site rates and the WAG evolutionary model. Tree visualized using the Python package etetoolkit (*65*) or ITOL (*66*).

Sequence analysis and structure prediction

Sequence alignment of KomA (VFT02523), KomB (VFT02524), and KomC (VFT02525) with their respective homologs was performed with Jalview (fig. S2) (*67*). Structures of the three proteins were predicted using AlphaFold3 (*68*). The predicted structures were aligned with the experimentally determined structures of their respective homologs using ChimeraX v1.8 (*69*).

To perform sequence logo analysis, all HAM1 protein sequences retrieved as described above were aligned using FAMSA v2.2.2 (*70*) with UPGMA tree mode, and the aligned fasta sequences were extracted separately for indicated clades. The sequence logo for each part was generated using Weblogo v3.7.12 (*71*) with chemistry color-scheme.

Genomic context analysis of ham1 genes

To determine whether a *ham1* gene is located within a defense island, known defense systems were identified using DefenseFinder v1.2.2 (*72*) and PADLOC v2.0.0 (*73*) within 20,000 bp upstream and downstream of the *ham1* gene. Then, the percentage of *ham*1 genes with defense systems located within ±20,000 bp was calculated for each specific HAM1 clade.

To analyze whether HAM1 is encoded near or in prophages and plasmids, the genetic elements were detected using the geNomad v1.8.0 (*74*) end-to-end pipeline within 75,000 bp upstream and downstream of the *ham1* gene. If prophages or plasmids were detected, the *ham1* genes were counted as being within or near mobile genetic elements.

To analyze the domains of the proteins encoded in ham1 neighborhood, hmmsearch is used to identify and annotate protein domains by comparing protein sequences against a library of HMM profile.

Spearman Analysis

The 16S rRNA phylogenetic tree was constructed for all organisms encoding defensive HAM1s, in which the 16S SSU rRNA, HAM1, and associated Sir2 genes were found. The 16S rRNA genes were identified via BLASTN v2.15.0+ searches (*75*), using the 16S rRNA sequence of *Escherichia coli* K-12 ER3413 as the query against bacterial genomes, with a word size of 8 and dust filtering disabled. Hits with at least 80% coverage and 70% identity were selected and aligned using MAFFT v7.525, and a phylogenetic tree was constructed using FastTree v2.1.11 with gamma-distributed site rates and the GTR evolutionary model. HAM1, and Sir2 protein sequences were aligned using MAFFT FFT-NS-1000, and approximate maximum-likelihood trees were generated using FastTree with gamma-distributed site rates and the WAG evolutionary model.

Statistics Analysis

For all statistics analysis, the assays were performed in three independent replicates as indicated in the figure legends, and the unpaired *t* test was used to calculate P values.

REFERENCES AND NOTES

1. F. Randow, J. D. MacMicking, L. C. James, Cellular self-defense: How cell-autonomous immunity protects against pathogens. *Science* **340**, 701–706 (2013). doi:10.1126/science.1233028 Medline
2. H. Georjon, A. Bernheim, The highly diverse antiphage defence systems of bacteria. *Nat. Rev. Microbiol.* **21**, 686–700 (2023). doi:10.1038/s41579-023-00934-x Medline
3. P. C. Ronald, B. Beutler, Plant and animal sensors of conserved microbial signatures. *Science* **330**, 1061–1064 (2010). doi:10.1126/science.1189468 Medline
4. S. J. Hobbs, P. J. Kranzusch, Nucleotide Immune Signaling in CBASS, Pycsar, Thoeris, and CRISPR Antiphage Defense. *Annu. Rev. Microbiol.* **78**, 255–276 (2024). doi:10.1146/annurev-micro-041222-024843 Medline
5. V. Hornung, R. Hartmann, A. Ablasser, K. P. Hopfner, OAS proteins and cGAS: Unifying concepts in sensing and responding to cytosolic nucleic acids. *Nat. Rev. Immunol.* **14**, 521–528 (2014). doi:10.1038/nri3719 Medline
6. F. Rousset, R. Sorek, The evolutionary success of regulated cell death in bacterial immunity. *Curr. Opin. Microbiol.* **74**, 102312 (2023). doi:10.1016/j.mib.2023.102312 Medline
7. K. Essuman, J. Milbrandt, J. L. Dangl, M. T. Nishimura, Shared TIR enzymatic functions regulate cell death and immunity across the tree of life. *Science* **377**, eabo0001 (2022). doi:10.1126/science.abo0001 Medline
8. O. Niewoehner, C. Garcia-Doval, J. T. Rostøl, C. Berk, F. Schwede, L. Bigler, J. Hall, L. A. Marraffini, M. Jinek, Type III CRISPR-Cas systems produce cyclic oligoadenylate second messengers. *Nature* **548**, 543–548 (2017). doi:10.1038/nature23467 Medline
9. M. Kazlauskiene, G. Kostiuk, Č. Venclovas, G. Tamulaitis, V. Siksnys, A cyclic oligonucleotide signaling pathway in type III CRISPR-Cas systems. *Science* **357**, 605–609 (2017). doi:10.1126/science.aao0100 Medline
10. D. Cohen, S. Melamed, A. Millman, G. Shulman, Y. Oppenheimer-Shaanan, A. Kacen, S. Doron, G. Amitai, R. Sorek, Cyclic GMP-AMP signalling protects bacteria against viral infection. *Nature* **574**, 691–695 (2019). doi:10.1038/s41586-019-1605-5 Medline
11. A. T. Whiteley, J. B. Eaglesham, C. C. de Oliveira Mann, B. R. Morehouse, B. Lowey, E. A. Nieminen, O. Danilchanka, D. S. King, A. S. Y. Lee, J. J. Mekalanos, P. J. Kranzusch, Bacterial cGAS-like enzymes synthesize diverse nucleotide

Downloaded from https://www.science.org at Shanghai Normal University on February 22, 2025

signals. *Nature* **567**, 194–199 (2019). doi:10.1038/s41586-019-0953-5 Medline
12. G. Ofir, E. Herbst, M. Baroz, D. Cohen, A. Millman, S. Doron, N. Tal, D. B. A. Malheiro, S. Malitsky, G. Amitai, R. Sorek, Antiviral activity of bacterial TIR domains via immune signalling molecules. *Nature* **600**, 116–120 (2021). doi:10.1038/s41586-021-04098-7 Medline
13. N. Tal, B. R. Morehouse, A. Millman, A. Stokar-Avihail, C. Avraham, T. Fedorenko, E. Yirmiya, E. Herbst, A. Brandis, T. Mehlman, Y. Oppenheimer-Shaanan, A. F. A. Keszei, S. Shao, G. Amitai, P. J. Kranzusch, R. Sorek, Cyclic CMP and cyclic UMP mediate bacterial immunity against phages. *Cell* **184**, 5728–5739.e16 (2021). doi:10.1016/j.cell.2021.09.031 Medline
14. K. S. Makarova, Y. I. Wolf, S. Snir, E. V. Koonin, Defense islands in bacterial and archaeal genomes and prediction of novel defense systems. *J. Bacteriol.* **193**, 6039–6056 (2011). doi:10.1128/JB.05535-11 Medline
15. S. Doron, S. Melamed, G. Ofir, A. Leavitt, A. Lopatina, M. Keren, G. Amitai, R. Sorek, Systematic discovery of antiphage defense systems in the microbial pangenome. *Science* **359**, eaar4120 (2018). doi:10.1126/science.aar4120 Medline
16. L. Gao, H. Altae-Tran, F. Böhning, K. S. Makarova, M. Segel, J. L. Schmid-Burgk, J. Koob, Y. I. Wolf, E. V. Koonin, F. Zhang, Diverse enzymatic activities mediate antiviral immunity in prokaryotes. *Science* **369**, 1077–1084 (2020). doi:10.1126/science.aba0372 Medline
17. A. Millman, S. Melamed, A. Leavitt, S. Doron, A. Bernheim, J. Hör, J. Garb, N. Bechon, A. Brandis, A. Lopatina, G. Ofir, D. Hochhauser, A. Stokar-Avihail, N. Tal, S. Sharir, M. Voichek, Z. Erez, J. L. N. Ferer, D. Dar, A. Kacen, G. Amitai, R. Sorek, An expanded arsenal of immune systems that protect bacteria from phages. *Cell Host Microbe* **30**, 1556–1569.e1555 (2022).
18. K. S. Makarova, Y. I. Wolf, J. van der Oost, E. V. Koonin, Prokaryotic homologs of Argonaute proteins are predicted to function as key components of a novel system of defense against mobile genetic elements. *Biol. Direct* **4**, 29 (2009). doi:10.1186/1745-6150-4-29 Medline
19. E. Koyuncu, H. G. Budayeva, Y. V. Miteva, D. P. Ricci, T. J. Silhavy, T. Shenk, I. M. Cristea, Sirtuins are evolutionarily conserved viral restriction factors. *mBio* **5**, e02249-14 (2014). doi:10.1128/mBio.02249-14 Medline
20. C. N. Vassallo, C. R. Doering, M. L. Littlehale, G. I. C. Teodoro, M. T. Laub, A functional selection reveals previously undetected anti-phage defence systems in the E. coli pangenome. *Nat. Microbiol.* **7**, 1568–1579 (2022). doi:10.1038/s41564-022-01219-4 Medline
21. D. K. Wilson, F. B. Rudolph, F. A. Quiocho, Atomic structure of adenosine deaminase complexed with a transition-state analog: Understanding catalysis and immunodeficiency mutations. *Science* **252**, 1278–1284 (1991). doi:10.1126/science.1925539 Medline
22. D. Ka, H. Oh, E. Park, J. H. Kim, E. Bae, Structural and functional evidence of bacterial antiphage protection by Thoeris defense system via NAD^+ degradation. *Nat. Commun.* **11**, 2816 (2020). doi:10.1038/s41467-020-16703-w Medline
23. A. Savchenko, M. Proudfoot, T. Skarina, A. Singer, O. Litvinova, R. Sanishvili, G. Brown, N. Chirgadze, A. F. Yakunin, Molecular basis of the antimutagenic activity of the house-cleaning inosine triphosphate pyrophosphatase RdgB from Escherichia coli. *J. Mol. Biol.* **374**, 1091–1103 (2007). doi:10.1016/j.jmb.2007.10.012 Medline
24. D. Mayo-Muñoz, R. Pinilla-Redondo, S. Camara-Wilpert, N. Birkholz, P. C. Fineran, Inhibitors of bacterial immune systems: Discovery, mechanisms and applications. *Nat. Rev. Genet.* **25**, 237–254 (2024). doi:10.1038/s41576-023-00676-9 Medline
25. A. Stokar-Avihail, T. Fedorenko, J. Hör, J. Garb, A. Leavitt, A. Millman, G. Shulman, N. Wojtania, S. Melamed, G. Amitai, R. Sorek, Discovery of phage determinants that confer sensitivity to bacterial immune systems. *Cell* **186**, 1863–1876 e1816 (2023).
26. G. S. Brush, S. K. Bhatnagar, M. J. Bessman, Bacteriophage T4 deoxynucleotide kinase: Gene cloning and enzyme purification. *J. Bacteriol.* **172**, 2935–2939 (1990). doi:10.1128/jb.172.6.2935-2939.1990 Medline
27. G. V. Mikoulinskaia, A. A. Zimin, S. A. Feofanov, A. I. Miroshnikov, Identification, cloning, and expression of bacteriophage T5 dnk gene encoding a broad specificity deoxyribonucleoside monophosphate kinase (EC 2.7.4.13). *Protein Expr. Purif.* **33**, 166–175 (2004). doi:10.1016/j.pep.2003.07.006 Medline
28. B. A. Adler, T. Hessler, B. F. Cress, A. Lahiri, V. K. Mutalik, R. Barrangou, J. Banfield, J. A. Doudna, Broad-spectrum CRISPR-Cas13a enables efficient phage genome editing. *Nat. Microbiol.* **7**, 1967–1979 (2022). doi:10.1038/s41564-022-01258-x Medline
29. J. Garb, A. Lopatina, A. Bernheim, M. Zaremba, V. Siksnys, S. Melamed, A. Leavitt, A. Millman, G. Amitai, R. Sorek, Multiple phage resistance systems inhibit infection via SIR2-dependent NAD^+ depletion. *Nat. Microbiol.* **7**, 1849–1856 (2022). doi:10.1038/s41564-022-01207-8 Medline
30. X. Song, S. Lei, S. Liu, Y. Liu, P. Fu, Z. Zeng, K. Yang, Y. Chen, M. Li, Q. She, W. Han, Catalytically inactive long prokaryotic Argonaute systems employ distinct effectors to confer immunity via abortive infection. *Nat. Commun.* **14**, 6970 (2023). doi:10.1038/s41467-023-42793-3 Medline
31. V. N. Noskov, K. Staak, P. V. Shcherbakova, S. G. Kozmin, K. Negishi, B.-C. Ono, H. Hayatsu, Y. I. Pavlov, HAM1, the gene controlling 6-N-hydroxylaminopurine sensitivity and mutagenesis in the yeast Saccharomyces cerevisiae. *Yeast* **12**, 17–29 (1996). doi:10.1002/(SICI)1097-0061(199601)12:1<17:AID-YEA875>3.0.CO;2-I Medline
32. N. Jia, R. Jones, G. Yang, O. Ouerfelli, D. J. Patel, CRISPR-Cas III-A Csm6 CARF Domain Is a Ring Nuclease Triggering Stepwise cA_4 Cleavage with ApA>p Formation Terminating RNase Activity. *Mol. Cell* **75**, 944–956.e6 (2019). doi:10.1016/j.molcel.2019.06.014 Medline
33. G. Cristalli, S. Costanzi, C. Lambertucci, G. Lupidi, S. Vittori, R. Volpini, E. Camaioni, Adenosine deaminase: Functional implications and different classes of inhibitors. *Med. Res. Rev.* **21**, 105–128 (2001). doi:10.1002/1098-1128(200103)21:2<105:AID-MED1002>3.0.CO;2-U Medline
34. N. S. Chandel, Nucleotide Metabolism. *Cold Spring Harb. Perspect. Biol.* **13**, a040592 (2021). doi:10.1101/cshperspect.a040592 Medline
35. J. S. Athukoralage, S. A. McMahon, C. Zhang, S. Grüschow, S. Graham, M. Krupovic, R. J. Whitaker, T. M. Gloster, M. F. White, An anti-CRISPR viral ring nuclease subverts type III CRISPR immunity. *Nature* **577**, 572–575 (2020). doi:10.1038/s41586-019-1909-5 Medline
36. S. J. Hobbs, T. Wein, A. Lu, B. R. Morehouse, J. Schnabel, A. Leavitt, E. Yirmiya, R. Sorek, P. J. Kranzusch, Phage anti-CBASS and anti-Pycsar nucleases subvert bacterial immunity. *Nature* **605**, 522–526 (2022). doi:10.1038/s41586-022-04716-y Medline
37. A. Leavitt, E. Yirmiya, G. Amitai, A. Lu, J. Garb, E. Herbst, B. R. Morehouse, S. J. Hobbs, S. P. Antine, Z. J. Sun, P. J. Kranzusch, R. Sorek, Viruses inhibit TIR gcADPR signalling to overcome bacterial defence. *Nature* **611**, 326–331 (2022). doi:10.1038/s41586-022-05375-9 Medline
38. E. Huiting, X. Cao, J. Ren, J. S. Athukoralage, Z. Luo, S. Silas, N. An, H. Carion, Y. Zhou, J. S. Fraser, Y. Feng, J. Bondy-Denomy, Bacteriophages inhibit and evade cGAS-like immune function in bacteria. *Cell* **186**, 864–876.e21 (2023). doi:10.1016/j.cell.2022.12.041 Medline
39. J. Davison, Pre-early functions of bacteriophage T5 and its relatives. *Bacteriophage* **5**, e1086500 (2015). doi:10.1080/21597081.2015.1086500 Medline
40. T. J. Mozer, H. R. Warner, Properties of deoxynucleoside 5′-monophosphatase induced by bacteriophage T5 after infection of Escherichia coli. *J. Virol.* **24**, 635–641 (1977). doi:10.1128/jvi.24.2.635-641.1977 Medline
41. H. Zhu, P. Smith, L. K. Wang, S. Shuman, Structure-function analysis of the 3′ phosphatase component of T4 polynucleotide kinase/phosphatase. *Virology* **366**, 126–136 (2007). doi:10.1016/j.virol.2007.03.059 Medline
42. D. J. McCorquodale, J. M. Buchanan, The T-odd bacteriophages. *CRC Crit. Rev. Microbiol.* **4**, 101–159 (1975). doi:10.3109/10408417509111574 Medline
43. D. Mayo-Muñoz, R. Pinilla-Redondo, N. Birkholz, P. C. Fineran, A host of armor: Prokaryotic immune strategies against mobile genetic elements. *Cell Rep.* **42**, 112672 (2023). doi:10.1016/j.celrep.2023.112672 Medline
44. Y. Gao, X. Luo, P. Li, Z. Li, F. Ye, S. Liu, P. Gao, Molecular basis of RADAR anti-phage supramolecular assemblies. *Cell* **186**, 999–1012.e20 (2023). doi:10.1016/j.cell.2023.01.026 Medline
45. B. Duncan-Lowey, N. Tal, A. G. Johnson, S. Rawson, M. L. Mayer, S. Doron, A.

Downloaded from https://www.science.org at Shanghai Normal University on February 22, 2025

Millman, S. Melamed, T. Fedorenko, A. Kacen, A. Brandis, T. Mehlman, G. Amitai, R. Sorek, P. J. Kranzusch, Cryo-EM structure of the RADAR supramolecular anti-phage defense complex. *Cell* **186**, 987–998.e15 (2023). doi:10.1016/j.cell.2023.01.012 Medline
46. J. Wu, L. Sun, X. Chen, F. Du, H. Shi, C. Chen, Z. J. Chen, Cyclic GMP-AMP is an endogenous second messenger in innate immune signaling by cytosolic DNA. *Science* **339**, 826–830 (2013). doi:10.1126/science.1229963 Medline
47. H. Chi, V. Hoikkala, S. Grüschow, S. Graham, S. Shirran, M. F. White, Antiviral type III CRISPR signalling via conjugation of ATP and SAM. *Nature* **622**, 826–833 (2023). doi:10.1038/s41586-023-06620-5 Medline
48. D. Sabonis, TIR domains produce histidine-ADPR conjugates as immune signaling molecules in bacteria. *BioRxiv*, (2024), doi: https://doi.org/10.1101/2024.01.03.573942; pmid
49. T. J. Mozer, R. B. Thompson, S. M. Berget, H. R. Warner, Isolation and characterization of a bacteriophage T5 mutant deficient in deoxynucleoside 5′-monophosphatase activity. *J. Virol.* **24**, 642–650 (1977). doi:10.1128/jvi.24.2.642-650.1977 Medline
50. T. Wein, R. Sorek, Bacterial origins of human cell-autonomous innate immune mechanisms. *Nat. Rev. Immunol.* **22**, 629–638 (2022). doi:10.1038/s41577-022-00705-4 Medline
51. M. A. Zamzami, Inosine Triphosphate Pyrophosphatase (ITPase): Functions, Mutations, Polymorphisms and Its Impact on Cancer Therapies. *Cells* **11**, 384 (2022). doi:10.3390/cells11030384 Medline
52. I. S. Waisertreiger, M. R. Menezes, J. Randazzo, Y. I. Pavlov, Elevated Levels of DNA Strand Breaks Induced by a Base Analog in the Human Cell Line with the P32T ITPA Variant. *J. Nucleic Acids* **2010**, 872180 (2010). doi:10.4061/2010/872180 Medline
53. E. Maffei, A. Shaidullina, M. Burkolter, Y. Heyer, F. Estermann, V. Druelle, P. Sauer, L. Willi, S. Michaelis, H. Hilbi, D. S. Thaler, A. Harms, Systematic exploration of Escherichia coli phage-host interactions with the BASEL phage collection. *PLOS Biol.* **19**, e3001424 (2021). doi:10.1371/journal.pbio.3001424 Medline
54. H. Li, R. Durbin, Fast and accurate short read alignment with Burrows-Wheeler transform. *Bioinformatics* **25**, 1754–1760 (2009). doi:10.1093/bioinformatics/btp324 Medline
55. P. Danecek, A. Auton, G. Abecasis, C. A. Albers, E. Banks, M. A. DePristo, R. E. Handsaker, G. Lunter, G. T. Marth, S. T. Sherry, G. McVean, R. Durbin; 1000 Genomes Project Analysis Group, The variant call format and VCFtools. *Bioinformatics* **27**, 2156–2158 (2011). doi:10.1093/bioinformatics/btr330 Medline
56. J. Cox, M. Mann, MaxQuant enables high peptide identification rates, individualized p.p.b.-range mass accuracies and proteome-wide protein quantification. *Nat. Biotechnol.* **26**, 1367–1372 (2008). doi:10.1038/nbt.1511 Medline
57. R. Cook, N. Brown, T. Redgwell, B. Rihtman, M. Barnes, M. Clokie, D. J. Stekel, J. Hobman, M. A. Jones, A. Millard, INfrastructure for a PHAge REference Database: Identification of Large-Scale Biases in the Current Collection of Cultured Phage Genomes. *Phage* **2**, 214–223 (2021). doi:10.1089/phage.2021.0007 Medline
58. S. C. Potter, A. Luciani, S. R. Eddy, Y. Park, R. Lopez, R. D. Finn, HMMER web server: 2018 update. *Nucleic Acids Res.* **46**, W200–W204 (2018). doi:10.1093/nar/gky448 Medline
59. L. Fu, B. Niu, Z. Zhu, S. Wu, W. Li, CD-HIT: Accelerated for clustering the next-generation sequencing data. *Bioinformatics* **28**, 3150–3152 (2012). doi:10.1093/bioinformatics/bts565 Medline
60. J. P. Meier-Kolthoff, M. Göker, VICTOR: Genome-based phylogeny and classification of prokaryotic viruses. *Bioinformatics* **33**, 3396–3404 (2017). doi:10.1093/bioinformatics/btx440 Medline
61. M. Steinegger, J. Söding, MMseqs2 enables sensitive protein sequence searching for the analysis of massive data sets. *Nat. Biotechnol.* **35**, 1026–1028 (2017). doi:10.1038/nbt.3988 Medline
62. M. N. Price, P. S. Dehal, A. P. Arkin, FastTree 2—Approximately maximum-likelihood trees for large alignments. *PLOS ONE* **5**, e9490 (2010). doi:10.1371/journal.pone.0009490 Medline
63. K. Katoh, K. Misawa, K. Kuma, T. Miyata, MAFFT: A novel method for rapid multiple sequence alignment based on fast Fourier transform. *Nucleic Acids Res.* **30**, 3059–3066 (2002). doi:10.1093/nar/gkf436 Medline
64. S. Capella-Gutiérrez, J. M. Silla-Martínez, T. Gabaldón, trimAl: A tool for automated alignment trimming in large-scale phylogenetic analyses. *Bioinformatics* **25**, 1972–1973 (2009). doi:10.1093/bioinformatics/btp348 Medline
65. J. Huerta-Cepas, F. Serra, P. Bork, ETE 3: Reconstruction, Analysis, and Visualization of Phylogenomic Data. *Mol. Biol. Evol.* **33**, 1635–1638 (2016). doi:10.1093/molbev/msw046 Medline
66. I. Letunic, P. Bork, Interactive Tree of Life (iTOL) v6: Recent updates to the phylogenetic tree display and annotation tool. *Nucleic Acids Res.* **52** (W1), W78–W82 (2024). doi:10.1093/nar/gkae268 Medline
67. M. Clamp, J. Cuff, S. M. Searle, G. J. Barton, The Jalview Java alignment editor. *Bioinformatics* **20**, 426–427 (2004). doi:10.1093/bioinformatics/btg430 Medline
68. J. Abramson, J. Adler, J. Dunger, R. Evans, T. Green, A. Pritzel, O. Ronneberger, L. Willmore, A. J. Ballard, J. Bambrick, S. W. Bodenstein, D. A. Evans, C.-C. Hung, M. O'Neill, D. Reiman, K. Tunyasuvunakool, Z. Wu, A. Žemgulytė, E. Arvaniti, C. Beattie, O. Bertolli, A. Bridgland, A. Cherepanov, M. Congreve, A. I. Cowen-Rivers, A. Cowie, M. Figurnov, F. B. Fuchs, H. Gladman, R. Jain, Y. A. Khan, C. M. R. Low, K. Perlin, A. Potapenko, P. Savy, S. Singh, A. Stecula, A. Thillaisundaram, C. Tong, S. Yakneen, E. D. Zhong, M. Zielinski, A. Žídek, V. Bapst, P. Kohli, M. Jaderberg, D. Hassabis, J. M. Jumper, Accurate structure prediction of biomolecular interactions with AlphaFold 3. *Nature* **630**, 493–500 (2024). doi:10.1038/s41586-024-07487-w Medline
69. E. C. Meng, T. D. Goddard, E. F. Pettersen, G. S. Couch, Z. J. Pearson, J. H. Morris, T. E. Ferrin, UCSF ChimeraX: Tools for structure building and analysis. *Protein Sci.* **32**, e4792 (2023). doi:10.1002/pro.4792 Medline
70. S. Deorowicz, A. Debudaj-Grabysz, A. Gudyś, FAMSA: Fast and accurate multiple sequence alignment of huge protein families. *Sci. Rep.* **6**, 33964 (2016). doi:10.1038/srep33964 Medline
71. G. E. Crooks, G. Hon, J. M. Chandonia, S. E. Brenner, WebLogo: A sequence logo generator. *Genome Res.* **14**, 1188–1190 (2004). doi:10.1101/gr.849004 Medline
72. F. Tesson, A. Hervé, E. Mordret, M. Touchon, C. d'Humières, J. Cury, A. Bernheim, Systematic and quantitative view of the antiviral arsenal of prokaryotes. *Nat. Commun.* **13**, 2561 (2022). doi:10.1038/s41467-022-30269-9 Medline
73. L. J. Payne, T. C. Todeschini, Y. Wu, B. J. Perry, C. W. Ronson, P. C. Fineran, F. L. Nobrega, S. A. Jackson, Identification and classification of antiviral defence systems in bacteria and archaea with PADLOC reveals new system types. *Nucleic Acids Res.* **49**, 10868–10878 (2021). doi:10.1093/nar/gkab883 Medline
74. A. P. Camargo, S. Roux, F. Schulz, M. Babinski, Y. Xu, B. Hu, P. S. G. Chain, S. Nayfach, N. C. Kyrpides, Identification of mobile genetic elements with geNomad. *Nat. Biotechnol.* **42**, 1303–1312 (2024). doi:10.1038/s41587-023-01953-y Medline
75. C. Camacho, G. Coulouris, V. Avagyan, N. Ma, J. Papadopoulos, K. Bealer, T. L. Madden, BLAST+: Architecture and applications. *BMC Bioinformatics* **10**, 421 (2009). doi:10.1186/1471-2105-10-421 Medline
76. Z. Zeng, Z. Hu, R. Zhao, J. Rao, M. Rodríguez Mestre, Y. Iiu, S. Liu, H. Feng, Y. Cheng, H. He, N. Chen, J. Zheng, D. Peng, M. Luo, Q. She, R. Pinilla-Redondo, W. Han, Base-modified nucleotides mediate immune signaling in bacteria, Zenodo (2025). doi:10.5281/zenodo.14837828

ACKNOWLEDGMENTS

We thank F. Wang at the National Key Laboratory of Agricultural Microbiology Core Facility, T. Liu and L. Zhong at the National Key Laboratory for Germplasm Innovation & Utilization of Horticultural Crops, D. Zhang at the core facilities of Center for Protein Research (CPR), and J. Li at Experimental Teaching Center of Bioengineering at Huazhong Agricultural University for assistance in HPLC, LC-MS, and protein purification. We thank S. Wu for providing Rao1 phage and A. Harms for providing BASEL collection. We thank S. J. Sørensen for generously granting us access to the laboratory space and

Downloaded from https://www.science.org at Shanghai Normal University on February 22, 2025

technical equipment at the Section of Microbiology, University of Copenhagen, Denmark. **Funding:** National Key Research and Development program of China 2022YFA0912200 (W.H.); National Natural Science Foundation of China 31970545 (W.H.); National Natural Science Foundation of China 32270099 (W.H.); Fundamental Research Funds for Central Universities 2662024SKPY003 (W.H.); Foundation of Hubei Hongshan Laboratory 2021hszd022 (W.H.); Hubei Special Project for Science Development 2024CSA060 (W.H.); Lundbeck Fonden grant R347-2020-2346 (R.P-R) VILLUM FONDEN VIL60763 (R.P.-R); Shandong University SKLMT Frontiers and Challenges Project SKLMTFCP-2023-01 (Q.S.). R.Z. is a recipient of CSC Scholarship. **Author contributions:** Conceptualization: Z.Z., R.P.-R, W.H.; Methodology: Z.Z., R.Z., J.R., H.H; Investigation: Z.Z., Z.H., R.Z., J.R., M.R.M, Y.L., S.L., H.F., Y.C., N.C., J.Z., D.P., M.L., Q.S., Visualization: Z.Z., R.Z.; Writing – original draft: Z.Z., R.P.-R, W.H.; Writing – review and editing: all authors; Funding acquisition: Q.S., R.P.-R, W.H.; Supervision: R.P.-R, W.H. **Competing interests:** W.H., Z.Z., Z.H., J.R., Y.L., and S.L. have submitted a patent application regarding the application of Kongming. The remaining authors declare that they have no competing interests. **Data and materials availability:** All data needed to evaluate the conclusions in the paper are present in the paper and/or the supplementary materials. All materials in this paper will be shared upon request. Codes can be found at Zenodo (*76*). Raw sequencing data are available in Sequence Read Archive (BioProject accession nos. PRJNA1149702 and PRJNA1195247). **License information:** Copyright © 2025 the authors, some rights reserved; exclusive licensee American Association for the Advancement of Science. No claim to original US government works. https://www.science.org/about/science-licenses-journal-article-reuse

SUPPLEMENTARY MATERIALS

science.org/doi/10.1126/science.ads6055
Figs. S1 to S19
Table S1 to S7
MDAR Reproducibility Checklist

Submitted 24 August 2024; accepted 11 February 2025
Published online 20 February 2025
10.1126/science.ads6055

Downloaded from https://www.science.org at Shanghai Normal University on February 22, 2025

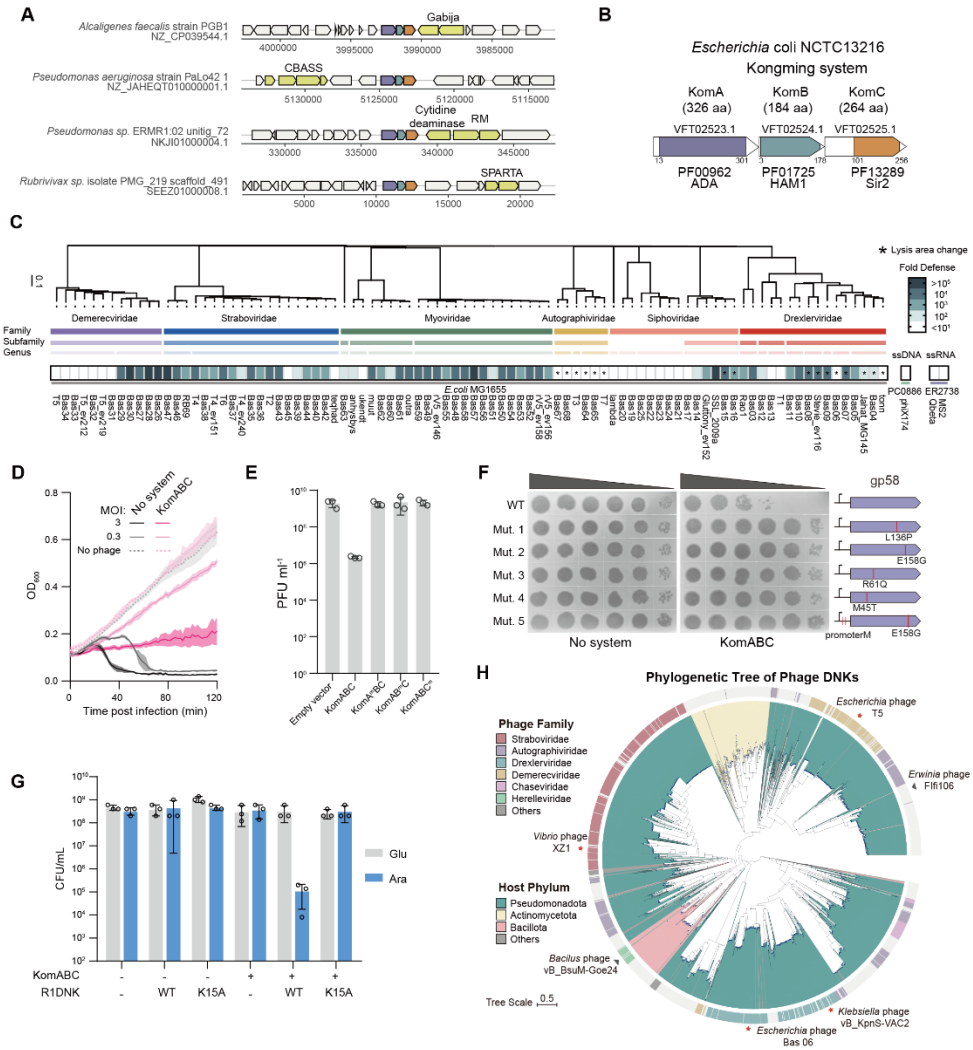


Fig. 1. Kongming is an anti-phage system that senses phage DNK. (**A**) A conserved three-gene operon is found in the neighborhood of known defense systems. Representative examples of the three-gene operon and their genomic contexts are shown. Known defense systems are highlighted in yellow. RM, restriction modification; CBASS, Cyclic oligonucleotide-based antiphage signaling system; SPARTA, short prokaryotic Argonaute TIR-APAZ system. The encoding strain and the respective DNA scaffold accession on the GenBank database are indicated. (**B**) Domain organization of the three-gene operon from *Escherichia coli* NCTC13216. ADA, adenosine deaminase domain; HAM1, HAM1-like non-canonical purine NTP pyrophosphatase domain. (**C**) Anti-phage activity of Kongming against a panel of 93 coliphages, showing the mean of three replicates. The branch lengths of the phage phylogenetic tree are scaled using the GBDP formula D0. Horizontal bars represent phages of the same taxonomic group up to the family level. ssDNA, single-stranded DNA; ssRNA, single-stranded RNA. (**D**) Growth curves of Kongming-expressing *E. coli* MG1655 (KomABC) and control strain (no system) post infection with the Rao1 phage at MOIs of 3 and 0.3. Data represent the mean ± SD of n = 3 biological replicates. (**E**) PFUs of Rao1 infecting *E. coli* MG1655 strains expressing wild-type or mutated KomABC (A^m, $KomA^{H15A-H17A}$; B^m, $KomB^{N9A-K12A-E15A}$; C^m, $KomC^{H146A}$). Data represent the mean ± SD of n = 3 biological replicates, with individual data points overlaid. (**F**) Rao1 mutants capable of escaping Kongming immunity carry mutations within the *gp58* gene. PFUs were analyzed for Rao1 and its escaper mutants on *E. coli* MG1655 expressing an empty vector (no system) or KomABC. Representative images of three independent replicates are shown. The mutations are represented on the right. Detailed information about the mutations is listed in table S5. WT, wild type. (**G**) R1DNK triggers cell death in the presence of KomABC. Colony forming units (CFUs) were measured for cells co-expressing KomABC and R1DNK or $R1DNK^{K15A}$ mutant on the plates containing glucose (Glu, to repress R1DNK expression) or arabinose (Ara, to induce R1DNK expression). Data represent the mean ± SD of n = 3 biological replicates, with individual data points overlaid. (**H**) Phylogenetic analysis of phage DNKs retrieved from the RefSeq complete phage genomes database (INPHARED). The names of phages encoding the experimentally tested DNKs in this work are indicated. Red star, coexpression of DNK and KomABC is toxic; black triangle, not toxic.

Downloaded from https://www.science.org at Shanghai Normal University on February 22, 2025

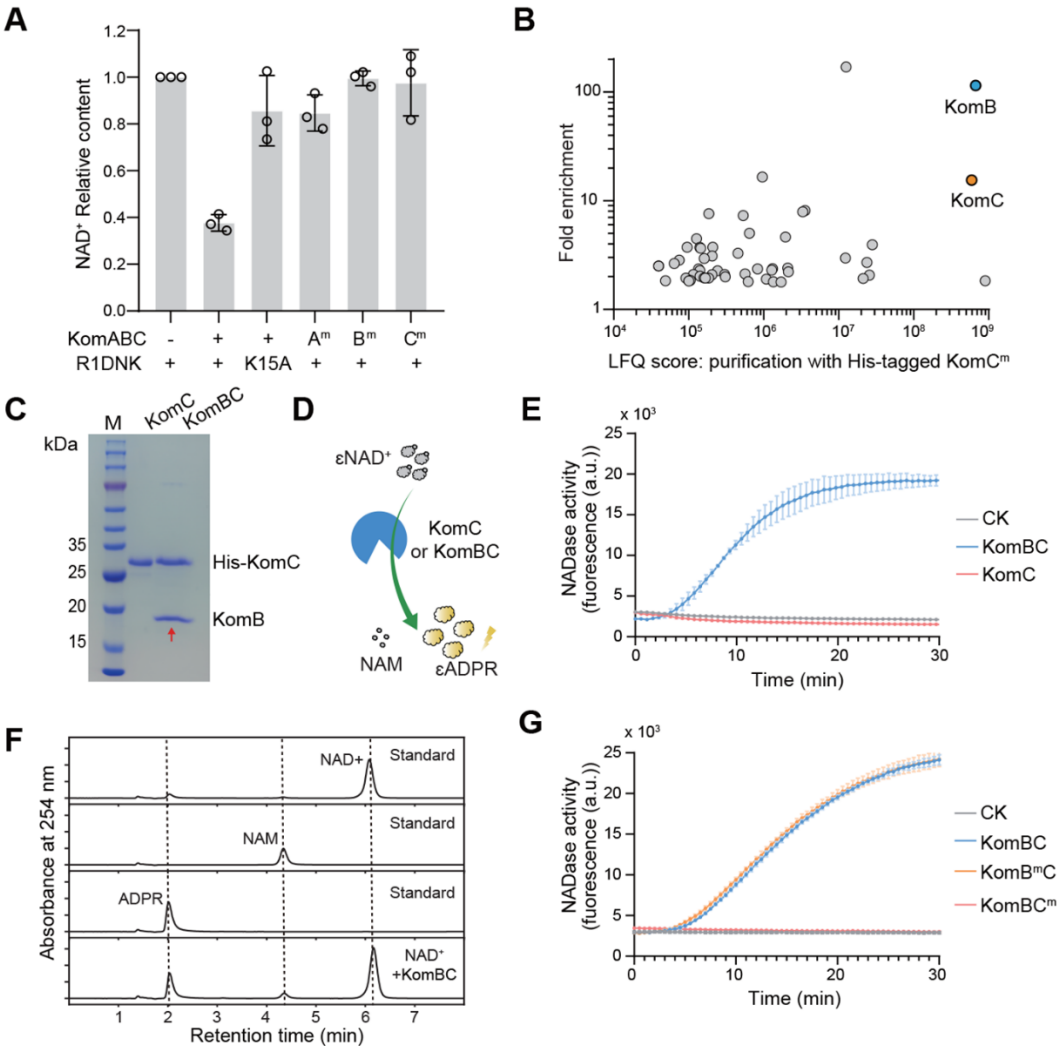


Fig. 2. KomB and KomC form an effector complex that mediates NAD⁺ depletion. (**A**) R1DNK triggers cellular NAD⁺ depletion in the presence of KomABC. NAD⁺ levels were measured for cells co-expressing KomABC and R1DNK, or their mutants: A^m, $KomA^{H15A-H17A}$; B^m, $KomB^{N9A-K12A-E15A}$; C^m, $KomC^{H146A}$. Data represent the mean ± SD of n = 3 biological replicates, with individual data points overlaid. (**B**) Mass spectrometry of the proteins purified from cells expressing KomA, KomB, His-tagged $KomC^{H146A}$ and R1DNK. Shown are the LFQ scores (*x* axis) and enrichment folds (*y* axis) compared to the sample purified from cells expressing KomA, KomB, untagged $KomC^{H146A}$ and R1DNK. Only the significantly enriched proteins are shown. KomB and KomC are indicated in the panel. (**C**) SDS-PAGE analysis of purified His-KomC and the KomB-(His)KomC complex (KomBC). The protein band indicated by the red arrow was validated to be KomB by mass spectrometry. (**D**) Schematic of the fluorogenic reaction used to analyze the NADase activity of KomBC and KomC. (**E**) NADase activity of purified 0.8 μM KomC and KomBC with ε-NAD as substrate. CK, reaction without any enzyme. Data represent the mean ± SD of n = 3 biological replicates. (**F**) HPLC analysis of the NAD⁺ degradation products of 0.1 μM KomBC, and NAD⁺, ADPR, and NAM as standards. (**G**) NADase activity of 0.6 μM KomBC and its mutants: B^m, $KomB^{N9A-K12A-E15A}$; C^m, $KomC^{H146A}$. CK, reaction without KomBC. Data represent the mean ± SD of n = 3 biological replicates.

Downloaded from https://www.science.org at Shanghai Normal University on February 22, 2025

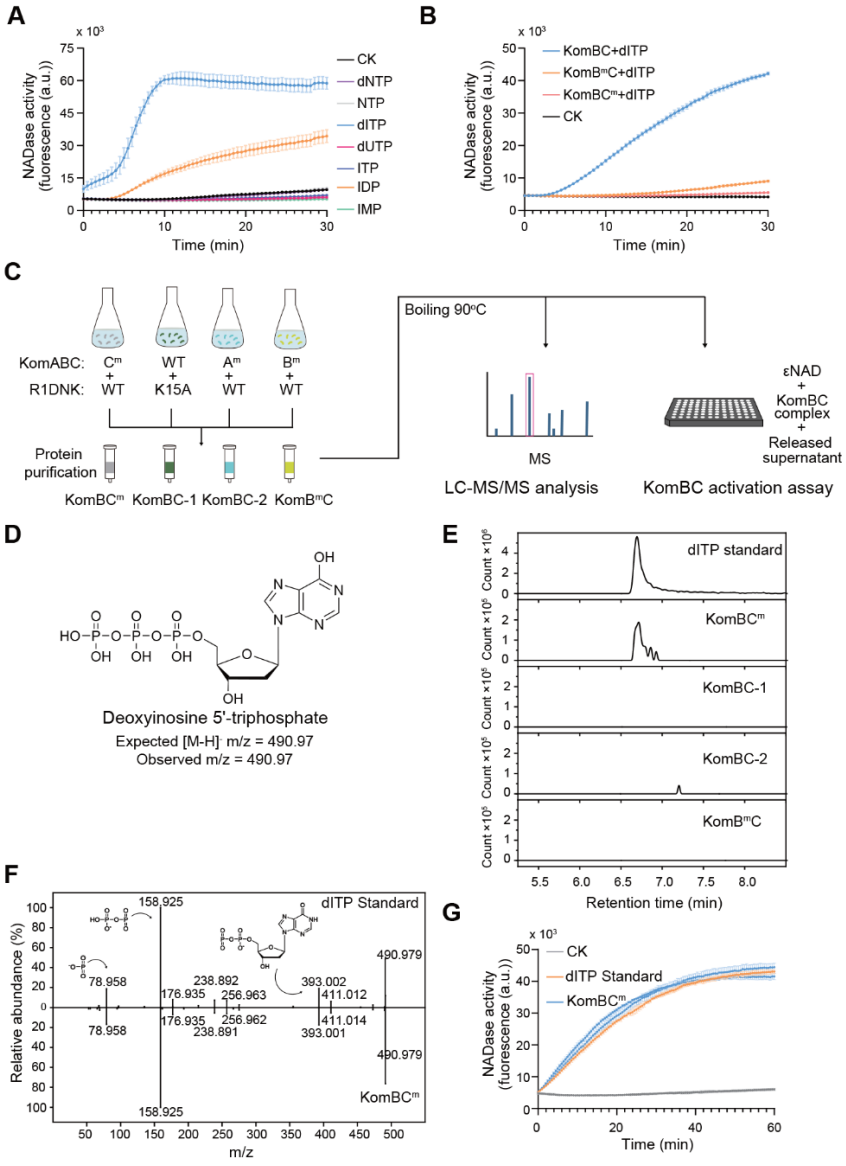


Fig. 3. dITP signaling activates the KomBC effector complex. (**A**) NADase activity of 50 nM KomBC in the presence of the indicated nucleotides. CK, reaction without any nucleotide. Data represent the mean ± SD of n = 3 biological replicates. (**B**) NADase activity of 50 nM KomBC and its mutants in the presence of dITP. CK, reaction without KomBC. Data represent the mean ± SD of n = 3 biological replicates. (**C**) Schematic representation of the experimental setup. The cells expressing mutated KomABC (A^m, $KomA^{H15A-H17A}$; B^m, $KomB^{N9A-K12A-E15A}$; C^m, $KomC^{H146A}$) and wild type R1DNK, or wild type KomABC and mutated R1DNK, were used for purification of different KomBC complexes. The complexes were subsequently denatured, and the released supernatants were analyzed by LC-MS/MS and tested for their ability to activate the NADase activity of wild type KomBC. (**D**) Chemical structure of dITP and its m/z value. (**E**) LC-MS analysis of the released supernatants from the denatured protein samples from (C). Extracted mass chromatograms of ions with an m/z value of 490.97 are presented. Shown are the representative data of two independent replicates. (**F**) MS/MS analysis of the released molecules from $KomBC^m$, using dITP as a standard. (**G**) NADase activity of 50 nM KomBC in the presence of the supernatant from $KomBC^m$, where the concentration of dITP was diluted to 1 nM. The experiments were performed in two independent replicates. dITP standard: 50 nM KomBC with 1 nM synthetic dITP; CK: 50 nM KomBC.

Downloaded from https://www.science.org at Shanghai Normal University on February 22, 2025

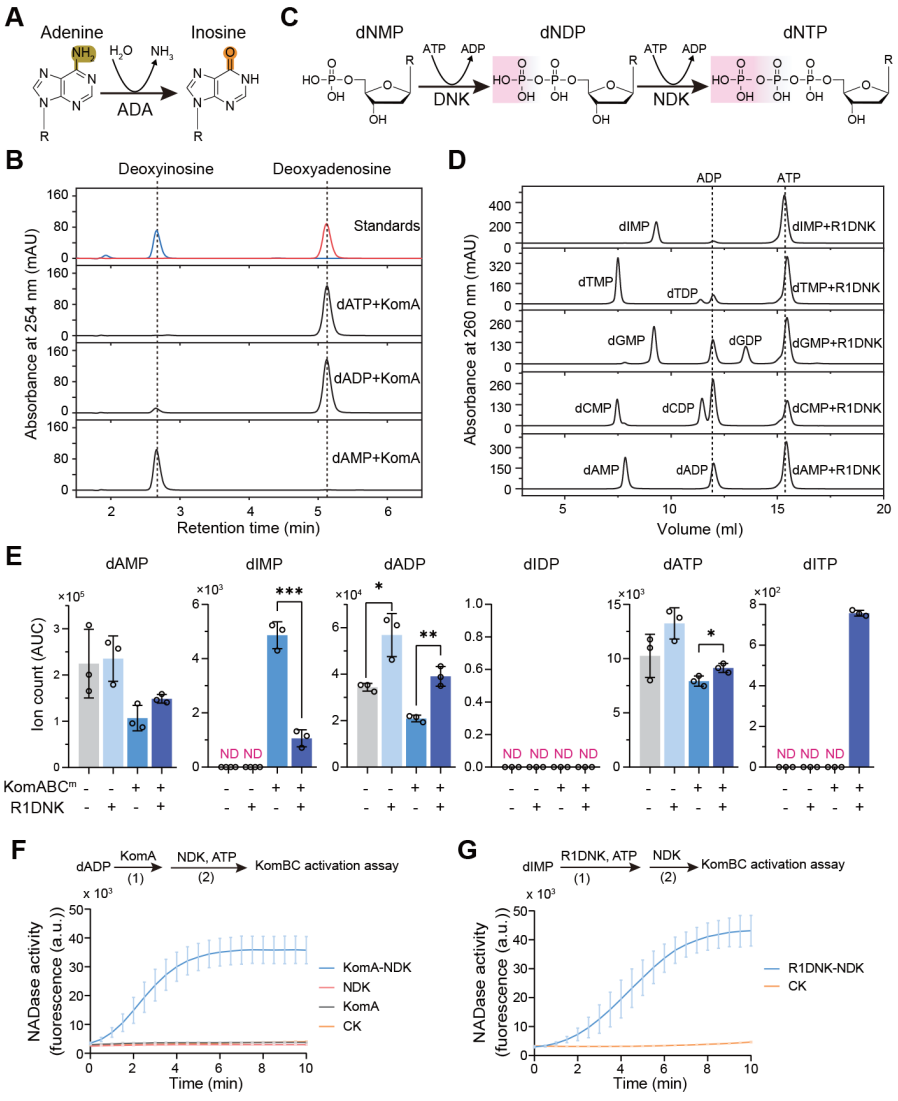


Fig. 4. Synthesis of the anti-phage signal dITP. (**A**) Schematic of the deamination reaction by typical adenosine deaminase enzymes (ADA). (**B**) HPLC analysis of the reactions of KomA using dATP, dADP, or dAMP as substrates. Deoxyadenosine and deoxyinosine were also analyzed by HPLC as standards. (**C**) Schematic of the phage dNTP synthesis pathway performed by phage DNK and host NDK, using dNMP as precursors. (**D**) Ion-exchange chromatography (IEC) analysis of the reactions of R1DNK with ATP as a phosphate donor and dIMP, dTMP, dGMP, dCMP, or dAMP as substrates. (**E**) Ion count (area under curve) of dAMP, dIMP, dADP, dIDP, dATP, and dITP in lysates extracted from cells expressing KomABC^m and/or R1DNK. Data represent the mean ± SD of n = 3 biological replicates, with individual data points overlaid. *P < 0.05; **P < 0.01; ***P < 0.001. ND, not detected. (**F**) NADase activity of 50 nM KomBC in the presence of the reaction product of KomA and NDK with dADP as substrate and ATP as phosphate donor. The reaction mixtures containing only KomA or NDK were also tested. CK: NADase activity of KomBC in the presence of dADP and ATP. Data represent the mean ± SD of n = 3 biological replicates. (**G**) NADase activity of 50 nM KomBC in the presence of the reaction product of R1DNK and NDK with dIMP as substrate and ATP as phosphate donor. CK, NADase activity of KomBC in the presence of dIMP and ATP. Data represent the mean ± SD of n = 3 biological replicates.

Downloaded from https://www.science.org at Shanghai Normal University on February 22, 2025

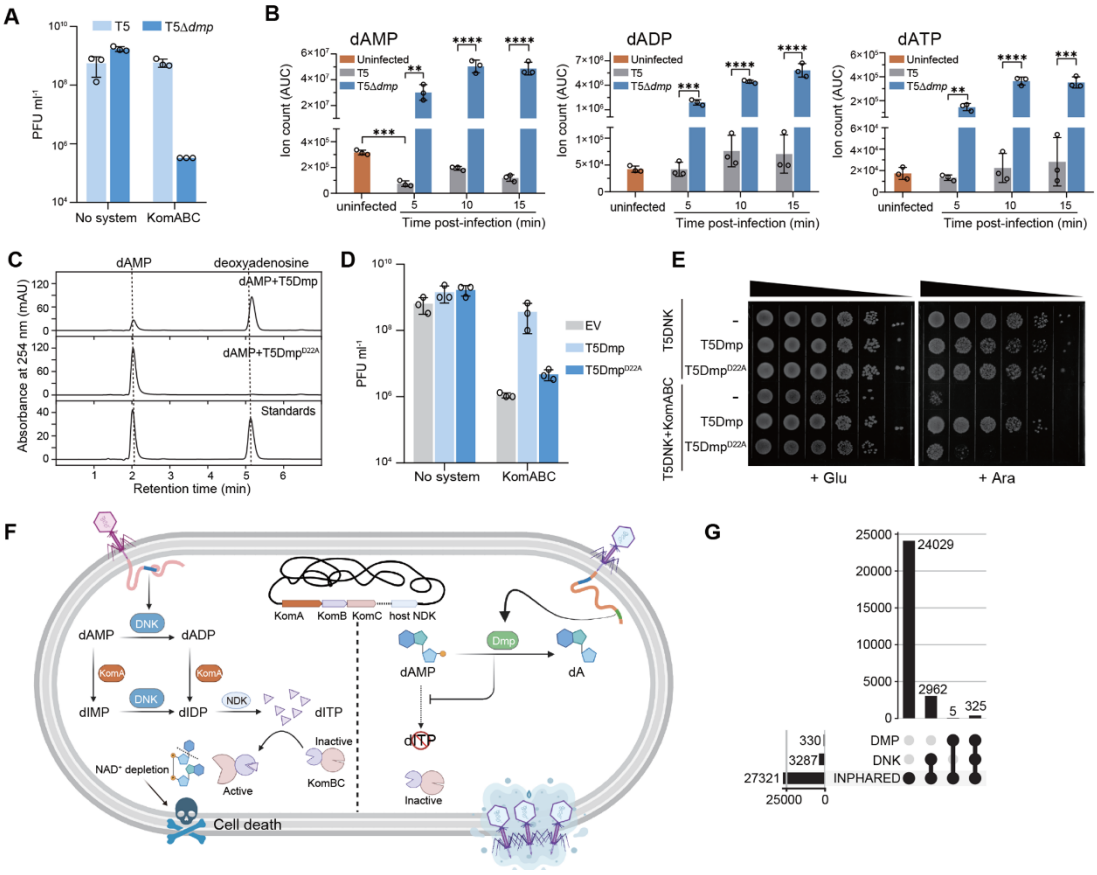


Fig. 5. T5 5'-deoxynucleotidase inhibits Kongming by degrading dAMP. (**A**) Deletion of *T5dmp* renders T5 sensitive to Kongming.PFUs were analyzed for T5 and the *dmp* deletion mutant on *E. coli* MG1655 lawns with or without KomABC. Data represent the mean ± SD of n = 3 biological replicates, with individual data points overlaid. (**B**) Ion count (area under curve) of dAMP, dADP, and dATP in lysates extracted from cells infected with T5 and $T5^{\Delta dmp}$, or uninfected cells. Data represent the mean ± SD of n = 3 biological replicates, with individual data points overlaid. $^{**}P < 0.01$; $^{***}P < 0.001$; $^{****}P < 0.0001$. (**C**) Mutation at the putative active site abolishes the dAMP phosphatase activity of T5Dmp. dAMP was incubated with T5Dmp or a D22A mutant, and the product was analyzed with HPLC. Deoxyadenosine and dAMP standards are shown at the bottom. (**D**) The D22A mutation abolishes the anti-Kongming function of T5Dmp. Cells expressing KomABC or not were transformed with an empty vector (EV) or plasmids encoding T5Dmp or its D22A mutant. Then, PFUs were analyzed for Rao1 infecting the bacterial lawns of the transformants. Data represent the mean ± standard deviation of n = 3 biological replicates, with individual data points overlaid. (**E**) T5Dmp inhibits the T5DNK-triggered toxicity in the cells expressing KomABC. Bacterial viability was measured for cells expressing KomABC, T5DNK, and T5Dmp or its D22A mutant on agar plates containing glucose (Glu, to repress T5DNK expression) or arabinose (Ara, to induce T5DNK expression). (**F**) (Left) The proposed model for the Kongming immune pathway. Phage DNK and KomA, together with host NDK, produce dITP as the signaling molecule using dAMP as precursor; then dITP activates the KomBC complex for NAD^+ depletion, resulting in death of the infected cells. (Right) The anti-Kongming function of phage-encoded Dmps. Phage Dmp degrades dAMP to dA (deoxyadenosine), thus inhibiting dITP synthesis. [Figure created with BioRender.com] (**G**) Correlation of phage-encoded DNKs and Dmps in phage genomes retrieved from the INPHARED database.

Downloaded from https://www.science.org at Shanghai Normal University on February 22, 2025

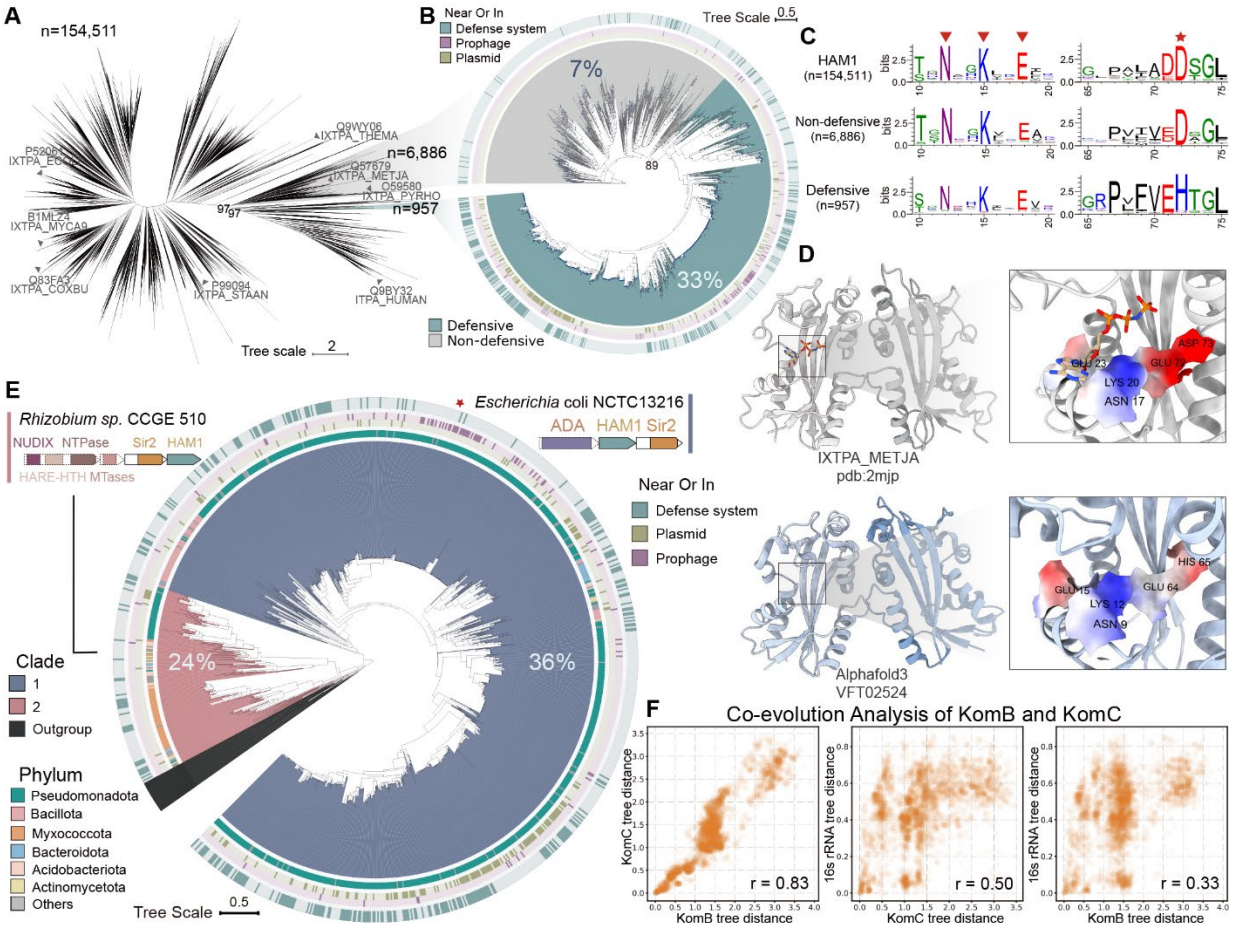


Fig. 6. Evolutionary analysis of Kongming components. (**A**) Phylogenetic tree of HAM1 domain-containing proteins. An unrooted tree was constructed using HAM1 domain-containing proteins from the non-redundant protein database, with sequences longer than 100 amino acids (n = 154,511). The sequence numbers of the two highlighted clades (gray and blue) are indicated. Local support values are shown for the indicated branches. Characterized housekeeping HAM1 proteins with experimentally determined structures are indicated with a gray arrow. (**B**) Phylogenetic tree of defensive and non-defensive HAM1s. All non-redundant sequences of defensive HAM1s were used, while only representative sequences of non-defensive HAM1s were included. For each clade, the percentage of HAM1s encoded near known defense systems is indicated. From outer to inner circles: whether each HAM1 is encoded near known defense systems, near or in prophages, and near or in plasmids. (**C**) Sequence logo representation of all, non-defensive and defensive HAM1s. Representative regions containing conserved substrate-binding residues (left) and the substitution of the catalytic aspartic acid by histidine in defensive HAM1s (right) are shown. (**D**) Structure comparison between a housekeeping HAM1 (IXTPA_METJA, PDB: 2mjp) and the AlphaFold3 structure (ipTM = 0.86, pTM = 0.87) of KomB. A close-up view of the substrate-binding area is shown with electrostatic surfaces of the residues indicated in (C). (**E**) Phylogenetic tree of defensive HAM1s. Twenty sequences of non-defensive HAM1s were used as an outgroup. The percentage of HAM1s encoded near known defense systems is indicated for each clade. Representative operons encoding HAM1 and Sir2 domains are shown. From outer to inner circles: whether each HAM1 is encoded near known defense systems, near or in prophages, near or in plasmids, and the bacterial phylum to which the HAM1 belongs. The red star indicates the HAM1 characterized in this study. (**F**) Spearman analysis (r, correlation coefficient) reveals strong co-evolutionary signal of KomB and KomC. The panels show plots of pairwise distances between KomB, the associated KomC, and the 16S rRNA of the organisms encoding the KomB and KomC, respectively. The Spearman rank correlation coefficient is indicated on each plot.

Downloaded from https://www.science.org at Shanghai Normal University on February 22, 2025